ELSEVIER

Contents lists available at ScienceDirect

Environmental Toxicology and Pharmacology

journal homepage: www.elsevier.com/locate/etap





High concentrations of Printex 90 carbon black ultrafine particles disturb the epithelial barrier in human primary respiratory mucosa models

Totta Ehret Kasemo^{a,*}, Maximilian Oppmann^b, Sofia Dembski^b, Maria Steinke^a, Elena Lajtha^a, Helena Moratin^a, Manuel Stöth^a, Agmal Scherzad^a, Mathilde Noémie Delaval^c, Ralf Zimmermann^{c,d}, Sebastiano Di Bucchianico^{c,d}, Stephan Hackenberg^a, Till J. Meyer^a

- ^a University Hospital Würzburg, Department of Oto-Rhino-Laryngology, Head and Neck Surgery, Würzburg, Germany
- ^b Fraunhofer Institute for Silicate Research ISC, Würzburg, Germany
- ^c Comprehensive Molecular Analytics (CMA), Helmholtz Zentrum München, Neuherberg, Germany
- d Institute of Chemistry, Department Life Light & Matter, University of Rostock, Rostock, Germany

ARTICLE INFO

Edited by Ayse Basak Engin

Keywords: Carbon black ultrafine particles respiratory mucosa primary cell model air-liquid interface toxicology barrier

ABSTRACT

Airborne pollutants harm human health, but the mechanisms involved remain unclear. Impaired epithelial barrier function is, as in respiratory diseases, one possible pathomechanism. To investigate this, carbon black (CB) as a model for ultrafine particles (UFP), was applied to respiratory mucosa models of primary fibroblasts and epithelial cells cultured at the air-liquid interface (ALI). Models were assessed for the mucociliary phenotype. Cytotoxicity, DNA damage, and barrier integrity were evaluated by the lactate dehydrogenase (LDH) and comet assays, and by transepithelial electrical resistance (TEER) measurements. Cilia movement and ultrastructure, secretory cells, and intact cell-cell contacts were confirmed. Subtle changes were observed: the LDH release had increased 2 h post exposure and barrier disturbance 24 h post exposure was detected, both without mucosal damage or genotoxic effects. Donor-specific differences were present. Barrier disruption without cell detachment or death suggests model feasibility for long-term studies of, e.g., tissue regeneration or fibrosis following UFP exposure.

1. Introduction

The harmful health effects of many airborne pollutants are well-described and increasingly central to environmental as well as health political discussions (Leikauf et al., 2020; Tainio et al., 2021; Peters et al., 2023). The pathophysiological mechanisms triggered by inhalable pollutants depend, among other parameters, on the particles' chemical and physical composition, and relate to their size. Particulate matter (PM), to which humans are exposed through various combustion and non-combustion sources, is typically categorized as PM_{0.1}, PM_{2.5} and PM₁₀, indicating single particle aerodynamic diameters smaller or equal

to $0.1~\mu m$ (ultrafine), $2.5~\mu m$ (fine) or $10~\mu m$ (coarse), respectively. $PM_{2.5}$ and PM_{10} cause increased mortality of circulatory diseases, lung cancer and other non-malignant respiratory diseases (World Health Organization, 2021). $PM_{0.1}$ or ultrafine particles (UFP) are components of these larger particle categories, often forming aggregates or agglomerates. However, the health impact of the UFP fraction remains poorly defined (Ohlwein et al., 2019; Stone et al., 2017; Vallabani et al., 2023). Theoretically, smaller particles with a greater surface area-to-volume ratio have a – relative to their mass – high potential to bind toxic molecules on their surfaces. The WHO has not yet published a risk assessment or specific recommendations for UFP but has issued good practice

Abbreviations: ALI, air-liquid interface; AECG-medium, Airway Epithelial Cell Growth Medium supplemented with P/S and provided supplements; BSA, bovine serum albumin; Caco, cacodylate; CK, cytokeratin; Des, desmosomes; DMSO, dimethyl sulfoxide; DdH2O, double distilled water; DMEM^{+ /+}, Dulbecco Modified Eagle's Essential Medium with FC and P/S; DLS, dynamic light scattering; EDTA, ethylenediaminetetraacetic acid; FC, Fetal Constance serum; H&E, hematoxylin and eosin; LDH, lactate dehydrogenase; MMS, methyl methanesulfonate; MUC, mucin; PM, Particulate matter; P/S, penicillin and streptomycin; PBS^{+/+}, phosphate buffer saline with Mg2 + and Ca2 +; PAHs, polycyclic hydrocarbons; PE, post exposure; CB, Printex 90 Carbon black particles; Rpm, revolutions per minute; RT, room temperature; TEER, transepithelial electrical resistance; TRIS, trishydroxymethylaminomethane; UFP, ultrafine particles; Z.A, zonula adherens; Z.O, zonula occludens.

^{*} Correspondence to: Josef-Schneider-Straße 11, Würzburg 97080, Germany. E-mail address: ehret t@ukw.de (T. Ehret Kasemo).

statements (World Health Organization, 2021) highlighting the potential health risks of UFP and the need for more data.

The respiratory mucosa, particularly in the upper airways, is the first point of contact with inhalable substances and thus requires special consideration in inhalation toxicology. Various studies report nasal deposition of "only" a small fraction of ultrafine particles and a somewhat higher percentage of larger particle deposition in the nose (Leopold, 1992). Kelly et al. used cast models to estimate deposition and conclude a deposition of $<10\,\%$ for particles $<30\,nm$ and over 10 % for larger UFPs (Kelly et al., 2004). Simulations suggest much less deposition in the nasal cavity, although particle number per cell has been suggested to be higher in the olfactory region than in alveoli (Chalvatzaki et al., 2025). For a number of reasons, nasal deposition and toxicology of UFP requires its own attention: 1) the nasal cavity has both veins and lymphatic vessels with the capacity to absorb and distribute xenobiotics such as particles. Some veins are fenestrated with the fenestrae always facing the apical side of the epithelium and, as a consequence, are potential entry points for xenobiotics. Lymphatic capillaries are distributed in the nasal cavity and are particularly prone to absorbing lipid soluble compounds. These are some of the reasons for the very high interest in the nose as an organ for drug delivery. A search for "nasal drug delivery" on PubMed reveals over 300 publications per year and rising since 2020 compared to 176 publications in the year 2012 (search performed on Oct. 19, 2025)). 2) The mucosal cell type composition in the nasal and bronchial niches differ (Deprez et al., 2020), which appears to have functional implications with differences in both gene expression and mucus content (Comer et al., 2012; Pohl et al., 2025; Stick et al., 2017). Hence, even though one niche may experience higher exposure, in order to understand which mechanisms are at play in response to particles, each niche should be considered separately. The differences to the lower airways and alveoli are even larger. 3) Interactions between particles and mucus are likely, even if particles eventually end up in the bronchi or lungs. Such interactions with mucins and their sugars or other molecules in mucus may manipulate the surface characteristics or agglomeration/accumulation behavior of particles and hence influence their toxicology in the lower airways; 4) estimates of nasal deposition are relatively general, i.e., usually not considering the amount or quality of mucus present, the variations of nostrils, nasal cavity geometries, such as the presence or absence of the supreme conchae (60-40 % distribution (Gizurarson, 2012) in the human population. As a consequence, certain groups (e.g. children or patients with nasal polyps) could have very different deposition patterns and it appears likely, that the estimates that are reported do not apply to all humans. 5) Particle number concentrations of UFP can be very high, so that even if a small fraction is deposited in the nose, high numbers of particles and a biological effect is perceivable; 6) UFPs accumulate and agglomerate and may stick as larger agglomerations in the nose to a larger extent than would be expected for "free" UFP. In addition to these arguments, it may be mentioned that some researchers argue for the possibility or observations of direct transport from the nose to the brain (Borisova and Komisarenko, 2021; Facciola et al., 2019; Song et al., 2015) through so called retrograde axonal transport (described by e.g. (Perlson et al., 2010)). Even though not finally clarified how or for all particle types, this possibility and its potentially severe consequences require attention due to the high risks such exposure would pose.

If there is harm to, *e.g.*, the nasal epithelium due to high or low nasal deposition doses, the integrity of the mucosal barrier is crucial for human resilience against the development or exacerbation of allergies, bacterial or viral infections, and chronic pulmonary diseases, such as asthma or chronic obstructive pulmonary disease (Aghapour et al., 2018; Yuksel and Turkeli, 2017). While UFPs have been associated with respiratory illnesses (Niranjan and Thakur, 2017), understanding for the underlying mechanisms remain incomplete. One reason is that different biological models – human volunteers, animals, cell lines or primary cell models and *ex vivo* tissue biopsies of different stages of differentiation and therefore correlation with actual human physiology – have been

used (Boland et al., 1999). In addition, research on the lungs and bronchi dominate over reports on the upper airways and the role of nasal deposition, uptake or potential barrier harm and inflammation remains unclear. The interdependence between trapping, filtering and alteration of particles in the nasal cavity, on the one hand, and the resulting exposure in the lower airways including alveoli, on the other hand, is also an important reason to clarify the role the nose plays in inhalation toxicology. Clarification of the above mentioned and other parameters will help improve in vitro mechanistic study design and interpretation of results also for models of bronchial or alveolar exposure. For a high in vivo-in vitro correlation of our study in the nasal mucosa, this work was designed to investigate UFP interactions with primary human tissue. Carbon black is an industrially produced soot widely used as an additive in tires and as a black color pigment. Benchmarked Printex 90 Carbon black particles (CB) were chosen due to their high level of standardization: they are produced under controlled conditions, are well-characterized carbon particles (>97 %) with a peak size of less than 100 nm (0.1 µm), and have commonly been used in in vitro particle studies (Lindner et al., 2017; Reisetter et al., 2011; Shen et al., 2018; Di Ianni et al., 2022).

Chaudhuri et al. reviewed CB genotoxicity and reproductive toxicity; (Chaudhuri et al., 2018). CB is poorly soluble and in its pure form considered to induce only low toxicity (see, e.g., (Jacobsen et al., 2008; Lindner et al., 2017). These authors conclude, that at high doses oxidative stress or inflammation may cause, as a secondary effect of CB exposure, mutations in the lungs and thereby have a genotoxic effect. In contrast, Di Ianni et al. question such associations between lung inflammation and genotoxicity, which, if at all existing would be a weak effect (Di Ianni, et al. 2022). Those authors rather argue that some strand break induction is possible, and that such damage could be a result of oxidative stress. Both reviews mainly rely on data from rodent exposures, or rodent-derived in vitro models, with some examples of human immortalized cell lines and human endothelial cells from the umbilical cord, and one example of human peripheral blood analyzed. A study using both cell lines and rodent models reported varying results depending on particle size and/or coating. Uncoated particles induced less IL-6 and IL-8 mRNA expression, whereas particle exposure generally led to decreased ciliary beat frequency and particle transport speed. Transepithelial electrical resistance (TEER) was determined in the Calu-3 cell line without any detected changes for CB (Lindner et al., 2017) although no absolute values were reported so that interpretation of those results is difficult. Unfortunately, the particle dose was reported as µg/ml without descriptions on the volume applied or the growth area for cells, so that no exposure mass per area estimation is possible, making dose comparisons difficult. Lindner et al. did report an effect of CB PAH coating, with, e.g., induction of IL-8 and apoptosis in the tracheal cell line. Apoptosis has also been described in alveolar macrophages in the form of pyroptosis (Reisetter et al., 2011). A different approach to test CB was taken by Shen et al., who investigated effects on mesenchymal stem cell capacity to differentiate after CB exposure. The authors reported impaired expression of osteogenesis markers as well as phenotypic impairment after in vitro induction of differentiation (Shen et al., 2018). As a proof of concept, those results suggest that also the basal (stem) cells of the respiratory mucosa could be functionally impaired in response to UFP or nanoparticles.

Here, a human primary cell-based model of the upper respiratory mucosa was used to investigate CB-associated cellular events. However, there is ongoing debate regarding the most suitable *in vitro* models for the toxicological and functional evaluation of airborne particles (Hiemstra et al., 2018; Jaber and Billet, 2024; Lacroix et al., 2018). On the one hand, air-liquid interface (ALI) models using cell lines are readily available and provide low variability in results. On the other hand, achieving a high *in vivo-in vitro* correlation in terms of morphology and functional aspects is only possible with the use of primary cells. Functional aspects such as the presence of mucus and beating kinocilia is crucial, as they are likely to influence both particle characteristics and

dynamics near cells. For example, particle retention time in mucus, and the corresponding potential for surface manipulation, can affect particle impacts on cells. This interaction is influenced by several factors, including mucus quality, thickness, and the movement caused by beating kinocilia. In addition, an intact epithelial barrier can be assumed to in turn influence mucus quality since a leaky barrier would, *e.g.*, add water and ions to the apical cell surface.

In vitro models that mimic these aspects likely have high translational value and are essential for generating data to aid in risk assessment in inhalation toxicology without exposing humans or animals in the long term. Since respiratory tract cell lines usually exhibit only some of these desired phenotypes, human primary respiratory cells and tissue models are regarded as valuable and more in vivo-like than cell line-based cultures to address respiratory research questions (Adcock et al., 2020; Lodes et al., 2020). A challenge with primary cell-based tissue models is that larger donor populations are desirable since donor variability is usually high in such models (Sivarajan et al., 2021) and can be expected to affect relevant inhalation study endpoints such as cytotoxicity, barrier integrity, or oxidative stress.

To get a more detailed understanding of potential human health impairments of UFP, the aim of the study was to evaluate the effects of the UFP model particle CB on human primary respiratory mucosa models. This included assessing CB size distribution, as well as its cytotoxic, genotoxic, and functional effects on respiratory models. Additionally, the study qualitatively examined the subcellular localization of the particles. Even though CB has been concluded previously to have low toxicity in cell lines and rodent models, the application in a primary cell based human model serves two major purposes: 1) establishing the here used human mucosal ALI model for inhalation research in general, and 2) including the epithelial barrier and possible disruption thereof as an endpoint in that setup. Since a non-intact barrier is more susceptible to both xenobiotics and pathogens, such damage would pose the future question of potential long-term effects of substances such as air pollutants, which are considered to be low in toxicity.

2. Materials and methods

2.1. Particles and particle characterization

CB (Printex 90) were prepared according to adjusted validated protocols from the NANoREG research project for in vitro and ecotoxicity studies (Boraschi, 2017). Briefly, particles were weighed and placed in sterilized, dry glass vials with screw caps. Endotoxin-free Bovine Serum Albumin (BSA) (Biomol, Hamburg, Germany) was dissolved (1 % w/v) in double distilled water (ddH2O) and stored at 4°C over night. On the day of exposure, the BSA-solution was sterile filtered (Minisart Syringe Filter High Flow, Sartorius, Göttingen, Germany). A small volume 98 % ethanol was added to the particles and the vial sealed for 1 min. Then, 0.05 % (v/v) BSA-water was added to a 2 mg/ml particle stock solution. Particles were then sonicated in an ice-cooled sonication bath (Sonorex TK 52, Bandelin electronic GmbH & Co. KG, Berlin, Germany) for $2\times15\,\text{min}$ with swirling the glass vial every 5 min. The stock suspension was diluted immediately before exposure to desired concentration volumes in Airway Epithelial Cell Growth Medium (PromoCell GmbH, Heidelberg, Germany) supplemented with 1 % Penicillin and Streptomycin (P/S) (Sigma-Aldrich, St. Louis, Missouri, USA) and provided supplements (AECG-medium) with a final concentration of 0.05 % of BSA. Since exposures (different concentrations) were carried out sequentially, the stock solution was sonicated again for 1 min before dilutions were performed after the first particle exposure.

The hydrodynamic diameter of CB was determined by dynamic light scattering (DLS) using a ZetaSizer ZS (Malvern Instruments, United Kingdom). The measurements were performed in a triplicate run with at least 12 measurements per run at 25 $^{\circ}$ C. The DLS laser had a wavelength of 633 nm and the scattered light was measured at 173 $^{\circ}$ in polystyrene cuvettes (No. 67.754, Sarstedt AG & Co. KG, Germany). The stock

suspension as well as particle dilutions were prepared as for experiments in cell culture medium and analyzed.

2.2. Isolation of primary cells and culture of respiratory mucosa models

Primary nasal respiratory tissue was obtained from 13 patients (SI 7), who underwent functional endoscopic sinus surgery or turbinoplasty. This study was approved by the Ethics Committee of the University of Würzburg (approval no. 116/17) and all patients gave informed consent to participate. Samples were processed no later than 4 h after surgery. To isolate epithelial cells, tissue samples were cleaned from cartilage, bone and blood and then sliced into approximately 1 mm³ tissue pieces in a dish using a sterile scalpel. After evenly distributing the pieces without medium in a new dish, they were covered and placed 5-10 min in the incubator to facilitate attachment. Then, 10 ml warm AECG-medium was carefully added to the side of the dish until tissue pieces were completely covered. During this step, it is important to avoid detachment of tissue pieces. Medium was then changed every 2-3 days. After 5–7 days, a sufficient number of epithelial cells has normally grown out of the tissue pieces, forming cell islands. Tissue pieces were removed on day 7 and used to isolate autologous fibroblasts by enzymatic digestion. The removed tissue pieces were processed according to previous protocols (Schweinlin et al., 2017). Briefly, after washing with $PBS^{Mg2+/Ca2+}$ ($PBS^{+/+}$) (Roche Diagnostics, Rotkreuz, Switzerland), pieces were cut into smaller pieces forming a sticky mass using a scalpel, and incubated (37 oC) with Collagenase-A-Solution (500 U/ml, Roche Diagnostics, Rotkreuz, Switzerland) on a shaker for 45 min - 1 h followed by centrifugation (270 x g) for 5 min at room temperature (RT). The cell pellet was resuspended in 10 ml Dulbecco Modified Eagle's Essential Medium (DMEM) (Thermo Fisher Scientific (Gibco), Waltham, MA, USA) with 10 % Fetal Constance serum (FC; # AC-SM-0190, anprotec, Brucksberg, Germany), generating DMEM+ (Linaris GmbH, Dossenheim, Germany) and 1 % P/S (DMEM+/+), then washed and centrifuged one more time. The remaining cell pellet was resuspended in 6 ml DMEM^{+/+} and cells were transferred to a T25 cell culture flask (Greiner, Kremsmünster, Austria) for culture.

To generate mucosa models, $1.12~\rm cm^2$ cell culture PET inserts were used with fibroblasts seeded in the basal compartment and epithelial cells in the apical compartment. Membrane inserts (pore size $0.4~\mu m$, 12-well, product number 3460, Corning Inc, Corning, NY, USA) were covered with 300 μ l Collagen A (1:1 solution with PBS^{+/+}; Collagen A, Biochrom GmbH, Berlin, Germany) and incubated at 37° C for 30 min – 1 h. Remaining collagen was removed by aspiration. Fibroblasts were prepared first. Cells were trypsinised [0.25 % Trypsin-EDTA, (1x; Thermo Fisher Scientific (Gibco)], washed in DMEM^{+/+}, and counted in a haemocytometer. 4×10^4 cells were added in 80 μ l DMEM^{+/+} on upside-down positioned inserts (basal compartment) and incubated for 2 h. Medium was then aspired, inserts rotated back and placed in 12-well plates (Corning, Inc., Corning, New York, USA). 1.5 ml warm co-culture-medium (1:1 mixture of AECG and DMEM^{+/+} 1:1) was added to each well.

Epithelial cells were detached from dishes by using 0.25 % trypsin-EDTA (1x) [Thermo Fisher Scientific (Gibco)] for 5–8 min using a cell scraper. Trypsin was inhibited by addition of DMEM $^{+/+}$ and cells were transferred to a 50 ml tube. After detachment, dishes were inspected to ensure that not too many cells were still attached. If needed, another scraping step in cell culture medium was performed. The cells were then centrifuged (270 x g, 5 min, RT). Supernatant was removed, 10 ml complete AECG medium added and a second centrifugation performed as before. Viable cells (determined by trypan blue staining) were counted using a haemocytometer.

On inserts with attaching fibroblasts in the basal compartment, 2×10^5 epithelial cells were seeded on the collagen-coated apical membrane side in 500 μl complete AECG medium. After 1–2 days (and 80–100 % confluent cells), all the media in the apical and the basolateral compartment was removed, and 1.5 ml of co-culture-medium was added

to the basolateral compartment. Models were cultured at the air-liquid interface (ALI) under standard cell culture conditions (37°C, 5 % CO₂) with medium change in the basolateral compartment 3 times per week. From day 7, an apical wash was performed along with each medium change as follows: $\sim\!500~\mu l$ PBS $^{+/+}$ was added using a pipet boy. The plate was incubated for 5–10 min followed by PBS-aspiration. From day $\sim\!25$ of ALI culture models were inspected for macroscopic appearance of mucus (this often also occurred earlier) and beating kinocilia using a light microscope using 20X and if needed 40X magnification. When both phenotypes were confirmed, experiments were carried out within $\sim\!1$ week, usually on ALI-culture day 28–45. For all experiments, donormatched fibroblasts and epithelial cells were used.

2.3. Exposures

For 12-well exposures, the Aeroneb® Lab Nebulizer system with 10 μ m pore-size (Aerogen, Galway, Ireland) has been evaluated for its dosimetry using zinc-oxide nanoparticles (158 nm primary particle diameter). The deposition was estimated to 68 % of the applied concentration for the conditions used in that study (Ding et al., 2020). Here, particle solutions for exposure were calculated to deposit as 0.01; 0.1; 1; 2; 4; and 8 μ g/cm² CB per insert/cell surface area with 100 % deposition. Our exposure chamber was made in-house, as described before (Meyer et al., 2023). Concentration calculations were adapted to the exact geometry of our chamber. Therefore, depositions can be estimated to 0.68* the concentrations given above, giving estimated true depositions of (rounded) ~0.007; 0.07; 0.7; 1.36; 2.7; and 5.4 μ g/cm² in this study.

For each exposure, the particle-medium suspension was added in 4 ml to the nebulizer and the nebulizer placed on the top of the chamber. The chamber with the cell culture plate was placed on a heating plate (37° C) in a safety flow cabinet. The nebulizer was run for 8 min until all liquid had been distributed in the chamber. Then, the chamber was left on the heating plate for another 35 min until no humid cloud could be seen. Under sterile conditions, the chamber top was removed and a medium-change of basal medium carried out. In cases of residual fluid other than on mucosa models (on plastic), these were aspirated. Exposed mucosa models were then placed in the incubator for post-exposure incubation. Negative controls were exposed to AECG with 0.05 % BSA-water only and otherwise treated as all other samples. Prior to each new particle concentration in one experiment, the nebulizer was washed with water and PBS⁺ and run with PBS⁺ in both directions to remove particle residues between exposures. Between each experiment (days), the nebulizer was sonicated in an ethanol bath and washed according to the producer's instructions.

2.4. Transepithelial electrical resistance (TEER) measurements

For each TEER-measurement, electrodes were sterilized and incubated in PBS⁺ prior to use. Measurements were performed with an EVOM2 (EVM-MT03-01, World Precision Instruments Ltd, Hertfordshire, United Kingdom) on a heating plate (37° C). 20 min prior to each 2 h post exposure (PE) endpoint, models were taken out, warm PBS⁺ was added apically and plates were placed back into the incubator. At 24 h PE, additionally the basal medium was changed 30–20 min prior to the measurement. The electrode was washed according to the manufacturer's instructions between different cell culture plates but not between model replicates for the same condition and same donor. A blank insert coated with collagen was measured on each measurement day and the value subtracted from other samples. The raw data was then normalized to the cell culture area (1.12 cm²) and visualized using the ggplot package (Wickham, H. (2016). ggplot2 - Elegant Graphics for Data Analysis Second Edition. Springer-Verlag New York. http://www.sprin ger.com/series/6991) in R Studio (Posit Team (2025). https://doi. org/10.1108/eb003648).

2.5. Lactate dehydrogenase (LDH) release analysis

A cytotoxicity detection kit (#11644793001, Roche) was used to analyze apically released LDH. After TEER measurements, (see above) $120~\mu l$ apical PBS $^{+/+}$ from each replicate was collected into tubes and placed on ice. Within 6 h, samples were centrifuged at 14 000 revolutions per minute (rpm) at 4° C and 2×50 µl supernatant from each replicate were carefully transferred into a 96-well plate. Dye solution and enzyme were mixed according to the manufacturer's instructions and added to samples using a multi-channel pipet and avoiding light exposure. The plate was analyzed in a Tecan reader (BioTek, Winooski, Vermont, USA) at 490 nm. A positive control in each experiment consisted of a mucosa model treated with 2 % Triton X-100 in PBS^{+/+}, which was added basally and apically. Upon addition of Triton X-100, models were mechanically disturbed with the pipet tip and Triton X-100slowly resuspended to ensure that Triton X-100 could cause total LDH release in all cells. Without this disturbance, models often appeared intact and no or little LDH could be measured in positive controls. Models were incubated for 2 h after adding the positive control. During analysis, a time-point at which the positive control reached an absorbance value of 2 (+/-0.1) was selected for data analysis. A PBS^{+/+} blank was measured and the value subtracted from all samples. All samples were normalized to the positive control, which was defined as 100 % LDH release.

2.6. Comet assay and cell count

The alkaline version of the comet assay (single cell gel electrophoresis) was performed to detect alkali labile sites, single strand breaks, and incomplete excision repair sites (Tice et al., 2000). Two or 24 h post exposure, epithelial cells were detached with 0.25 % trypsin-EDTA and scraping with the pipet tip. Treatment with 500 μM alkylating agent methyl methanesulfonate (MMS, # 129925-5 G, Sigma-Aldrich (Merck), Darmstadt, Germany) for 2 h served as positive control. Cells were collected in 1.5 ml tubes and centrifuged at 4° C (270 x g, 5 min). Supernatant was aspired and 500 µl freezing medium added (50 % FC, 40 % AECG, and 10 % dimethyl sulfoxide (DMSO; # 47202, Carl Roth, Karlsruhe, Germany) (v/v)). Cells were frozen in freezing blocks to -80°C for 24 h and stored until analysis. For the assay, cells were thawed, washed and counted in a haemocytometer with trypan blue staining to determine the fraction of viable cells. Prior to analysis, glass slides were prepared by coating with 1.5 % agarose (05066-50 G, Sigma-Aldrich) in $PBS^{+/+}$. Cells were then suspended in 0.5 % low melting point agarose (A9414-10G, Sigma-Aldrich (Merck), Darmstadt, Germany). Eight droplets of 20 µl cell suspension (1250 cells/ droplet) were transferred to a coated glass slide (#03-0014/45, R. Langenbrinck GmbH, Emmendingen, Germany), and covered by plastic foil. Next, cells were lysed by incubation for 1.5 h in alkaline lysis buffer (10 % DMSO, 1 % Triton X-100, 2.5 M NaCl, 10 mM tris(hydroxymethyl)aminomethane (TRIS; Trizma base, Sigma-Aldrich (Merck), Darmstadt, Germany), 100 mM Na₂-Ethylenediaminetetraacetic acid (EDTA; #ED2SS-1KG, Sigma-Aldrich (Merck), Darmstadt, Germany), pH 10). The gel electrophoresis was performed in a horizontal dark gel electrophoresis chamber on ice (in-house design) with alkaline buffer (5 mM NaOH (#1375.1000, Th. Geyer, Renningen, Germany) and 200 mM Na₂EDTA) at pH > 13. First, 20 min DNA unwinding was performed, then 20 min electrophoresis with 300 mA and 0.8 V/cm. The pH was neutralized by TRIS-buffer and the cells fixed with cooled $(-20 \circ C)$ methanol (#32213-2.5L-M, Sigma-Aldrich (Merck), Darmstadt, Germany) and allowed to dry overnight. Subsequently, the cells were stained by adding 20 µl of GelRed (Biotium Inc., Fremont, CA, USA) and covered with a cover glass for microscopic analysis. Comets were detected on a Leica DM4000 B (Leica, Wetzlar, Germany) and analyzed using Komet 5.5 (Kinetic Imaging Ltd, Nottingham, UK).

2.7. Cytokine quantification by bead assay

Released cytokines in supernatants were quantified in technical duplicates using an antibody-coupled bead assay (LEGENDplex Human Anti-Virus Response Panel Mix and Match Subpanel; #740356 IL6 Capture Bead A5, #740357 IL-8 Capture Bead A10, #740358 IL-10 Capture Beads B7, #740359 TNF-alpha Capture Bead B6, #740119 IL-1ß Capture Bead A4, #740365 Human Anti-Virus Response Panel Standard, #740364 Human Anti-Virus Response Panel Detection Antibodies; BioLegend (Lehmann et al., 2019), San Diego, California, USA) and detected using a flow cytometer (FACS Canto, BD Biosciences, Franklin Lakes, New Jersey, USA). For each experiment, at least one positive control was included consisting of total intracellular plus extracellular cytokines retrieved by 2 h incubation with 2 % Triton X-100 (Sigma-Aldrich, (Merck), Darmstadt, Germany) in PBS^{+/+}. For the assay, a supplied standard for each cytokine was included in duplicates with a maximum concentration of $\sim 7-9*10^4$ pg/ml (exact concentrations are defined for each bead-population by the provider and made available in the certificate for each kit). Data analysis and cytokine quantification was based on standard curves and performed using the online platform Qognit provided by the kit provider (BioLegend). Averages of technical duplicates are shown.

2.8. Histology – paraffin and H&E staining

At indicated time-points, samples were washed with PBS $^{+/+}$ and fixed in 4 % formaldehyde (Roti®-Histofix, Carl Roth, Karlsruhe, Germany) for 1.5–3 h (apical and basal application). After fixation, the samples were washed 2x in PBS $^{+/+}$ and then stored in PBS $^{+/+}$ until further processing. For dehydration, membranes were cut out of inserts using a scalpel. Membranes were then cut in the middle and embedded in paraffin by hand. Paraffin blocks were cut in 5 μ m sections and placed on glass slides. Xylene and descending ethanol series were used for rehydration. Staining with hematoxylin and eosin (H&E) was performed according standard protocols. Sections were visualized using a microscope (BZ-X800, Keyence, Osaka, Japan). Selected images are shown in supplementary information (SI) 3.

2.9. Antibody staining of model sections

Prior to antibody staining, 10 μm sections of paraffin embedded culture inserts were de-masked for epitope retrieval using a steamer (slides and buffers cooked at 100°C for 10 min) at pH 9 (TRIS/EDTA-Buffer) for anti-cytokeratin (CK) 5 and acetylated- α -tubulin and at pH 6 (Citrate-Buffer) for anti-mucin (MUC) 5AC and MUC5B. Antibodies, their target cells/structures, sources and dilutions used are indicated in Table 1. Imaging was performed using a Leica DMi8 (Microscope) and Leica DFC 3000 G (Camera).

2.10. Transmission electron microscopy

For electron microscopy, models were washed in PBS $^{+/+}$. Then, 2.5 % glutaraldehyde in 0.05 M cacodylate (caco) buffer was added apically and basally and models were fixed for 2–3 h at RT. After fixation, models were washed 5 times for 3 min with caco-buffer and then stored in caco-buffer for transport to Würzburg University's Imaging Core Facility for further processing. Further processing was done after a maximum of 2–3 days (at 4° C). Briefly, models were washed in 50 mM caco-buffer (pH 7.2) and fixed in 2 % OsO₄. After washing in H₂O, models were stained with 0.5 % uranyl acetate and then dehydrated in rising ethanol series (50 %, 70 %, 90 % and 100 %) followed by propylene oxide. At the end, models were kept in 100 % ethanol for 30 min at RT and then in propylene oxide for 30 min. Samples were treated with Epon 812 / propylene oxide (1:1) over night. Then, samples were embedded in Epon 812 for 2 h and then stored at 60°C for at least 48 h for polymerization. Sections were contrasted with 2 % uranyl acetate in

Table 1Overview of antibodies and staining dilutions for immunofluorescence assay of murosa model sections

Target protein/ Structure	Target structure	Primary Antibody/Dye and dilution	Secondary Antibody and dilution	Reference
CK5	Basal cells	Anti- Cytokeratin 5/ 6, mouse [Agilent (Dako); Ref. #: M72371 1:200	A647 donkey anti-mouse [Thermo Fisher, Ref. #: A32787] 1:1000	(Lodes et al., 2020)
Acetylated- α-tubulin	Kinocilia/ differentiated ciliated cells	Acetylated- α-tubulin (Lys40), rabbit [Cell Signaling; Ref. #: 5335] 1:300	A555 donkey anti-rabbit [Thermo Fisher, Ref. #: A32794] 1:1000	(Mao et al., 2018)
MUC 5AC	Mucin/mucus/ Goblet cells	MUC5AC, mouse [Invitrogen; Ref. #: MA5–12178] 1:1000	A647 donkey anti-mouse [Thermo Fisher, Ref. #: A32787] 1:1000	(Lodes et al., 2020)
MUC 5B	Mucin/mucus/ Goblet cells	MUC5B, rabbit [Sigma; Ref.#: HPA008246] 1:500	A555 donkey anti-rabbit [Thermo Fisher, Ref. #: A32794] 1:1000	(Lodes et al., 2020)
Nucleus	Adenine/ Thymine-rich DNA	Fluoromount-G with DAPI [Invitrogen; Ref. #: 004959–52]	4',6- diamidino-2- phenylindole (DAPI) – update- ready- solution used	-

ethanol (Reynold's lead citrate solution) (or left uncontrasted where indicated). Imaging was performed at the Imaging Core Facility, Würzburg University using a JEOL JEM-1400 Flash for higher resolution (e.g. particle visualization).

2.11. Statistics

Data were collected in standard spreadsheets and imported into R, build 369, released on 2023-12-17 ("R Development Core Team," 2008). In total, 13 donors were included and in analyses for which statistical tests were carried out, at least 5 donors were represented. Not all donors were included in all assays. Color-coding in figures indicate individual donors and is consistent throughout the manuscript. For TEER-data, negative control data collected on other time-points than the experimental day were excluded (removed: 156 data points). Donors/ samples, which were generated during pilot experiments and only exposed to 1-2 conditions, were also excluded, since their influence on the variance sometimes was high without a possibility to determine the role of donor-specific tendencies (generally high/low for specific donors) or concentration-dependencies. A student's t-test was applied ("Welch Two Sample Test", RStudio) where indicated. In a small number of cases, datapoints were excluded after finalizing experiments/during data analysis, if the donor was not represented in negative control or not in > 3 concentrations. Of particular importance were instances, in which negative controls from each donor were missing. This is important due to the observed donor variability, since the lack of such controls do not allow qualitative assessment/analysis for reasons of outliers in the experimental groups.

3. Results

3.1. Morphology of differentiated airway mucosa models

Airway mucosa models were generated from human nasal tissue biopsies by isolating epithelial cells and fibroblasts separately. Donors were 50 % males (average age 52 years) and 50 % females (average age 39 years; see SI 1). Grown on collagen-coated polyester membranes in co-culture with fibroblasts, epithelial cells differentiated for several weeks (usually ~28-45 days) to the mucociliary phenotype. Beating kinocilia were confirmed with light microscopy and mucus production could be seen macroscopically by the bare eye (see macroscopic view of exposed cell culture plate in SI 2). The models stain positive for cytokeratin (CK) 5, indicating the maintenance of a stem cell niche in the cultures (Fig. 1). Epithelial cell differentiation was confirmed by H&E staining of sectioned models (SI 3) and positive staining for acetylated $\alpha\text{-tubulin}$ for ciliated cells, and mucins 5AC and 5B verify the presence of goblet/secretory cells (negative controls for secondary antibodies are shown in SI 4). Ultrastructural analysis with TEM confirmed kinocilia with $9 \times 2 + 2$ microtubuli-structure and cells with goblet cell-similar morphology, as well as cell-cell contacts, such as tight junctions/zonula occludens (Z.O.), adherens junctions/zonula adherens (Z.A.) and desmosomes (Des.) (Fig. 2) (Fig. 3).

3.2. Carbon black characterization

For control of the expected particle size, CB was prepared in double-distilled water, sonicated, and measured three times consecutively by DLS. Alternatively, particles were diluted in cell culture medium with BSA post sonication to the experimental concentrations and measured 3 times consecutively. The DLS measurement data obtained are summarized in Table 2, the cumulative number distributions are shown in Figure SI 5. The analysis of the DLS measurement data resulted in a hydrodynamic diameter of 77 ± 22 nm for the CB dispersed in double distilled water (Table 2). This corresponds well with the expected value of ≈ 70 nm. When particles were diluted in cell culture medium as for experiments and measured approximately 1, 3, and 5 min after sonication and dilution, the calculated hydrodynamic diameters increased for all concentrations, compared to the sample in water. The increased

hydrodynamic diameters can be attributed to an increase in the hydration shell due to the presence of salts and cell medium supplements. The deviations between the concentrations were within the calculated error limits of the hydrodynamic diameters. Since no concentration-dependent size-differences in cell culture medium were observed within the investigated time frame, particles with comparable size distributions were used for all tested concentrations. Furthermore, primary particle grain sizes and morphology by TEM are exemplified in Fig. 2 at different magnifications in B-D (A: negative control of water only). Primary grain sizes between ~15 and 50 nm can be seen, confirming the ultrafine/nanoparticle nature of the CB used in this study.

3.3. LDH-release in response to CB

During TEER measurements, (see below) apical PBS is added to cultures for approximately 30 min. This supernatant or "apical wash" from treated and control models was analyzed for LDH release, a wellestablished indicator of cytotoxicity that does not consume the models or disturb cells. The same technical replicates could therefore be analyzed by TEER and/or partly in the comet assay (see donor ID indications in figures). As positive control, complete tissue models were treated with Triton X-100 and the total LDH released was defined as 100 % for each donor. After 2 h, 4 µg/cm² exposure induced the highest LDH-release with a donor average in the NC of 9.3 % of the positive control (PC) and 17.5 % in the exposed samples (Welch's t-test p-value = 0.012, n = 4-5 donors), which was not reflected at 8 μ g/cm². Nevertheless, an LDH release of 20 % or less is generally not considered indicative of cytotoxicity. The significant increase below this threshold could be an indication of membrane damage without cell death. At 8 µg/ cm², one donor exhibited a higher release, but the average was the lowest among all particle exposed groups. Data from 3 donors after 24 h indicate more donor variance in cytotoxicity at this time-point. All NC remained below 25 % LDH-release relative to the PC even at 24 h PE (no statistics were performed due to low number of donor replicates).

3.4. No acute genotoxicity-response to CB

Frozen cells after exposures were thawed and the alkaline single cell gel electrophoresis (comet assay) was conducted to assess DNA damage.

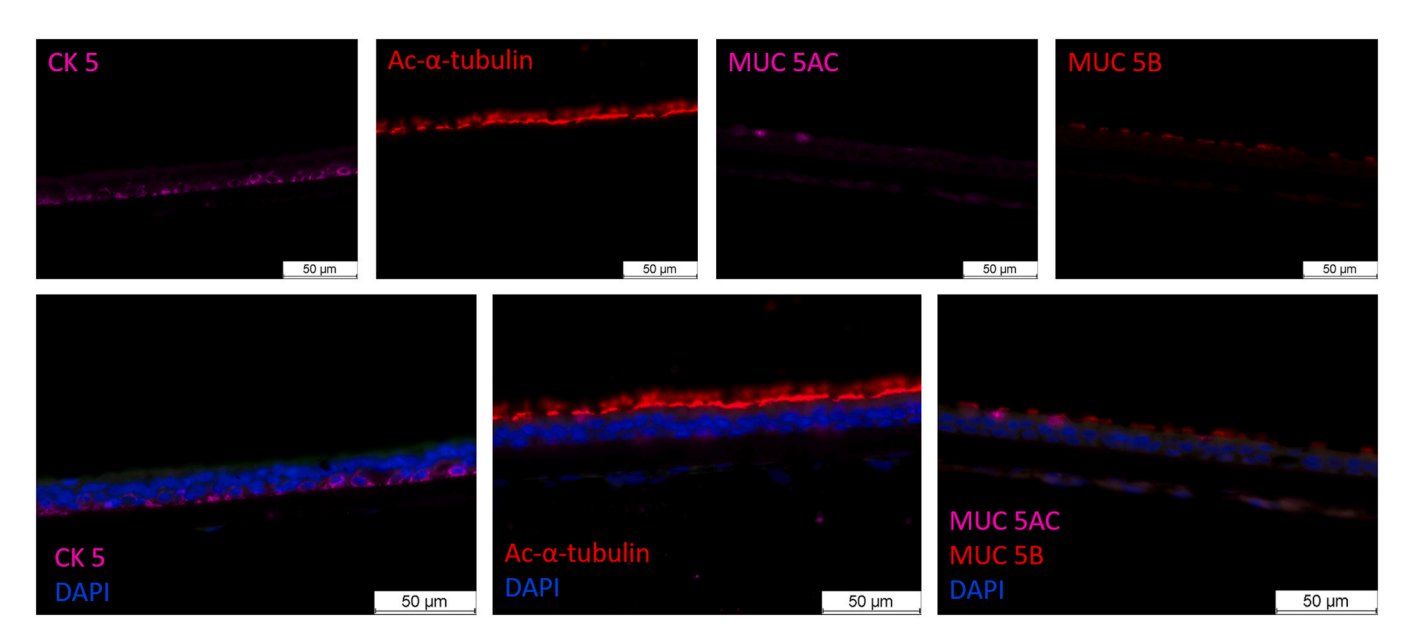


Fig. 1. Immunofluorescent staining of paraffin sections of mucosa models. Antibodies used and their color are indicated in the images. CK5 marks basal cells, Acetylated-α-tubulin (Ac-α-tubulin) binds to microtubule structures in kinocilia, MUC5AC and MUC5B bind their respective mucins and can hence label both goblet/secretory cells and extracellular mucus. DAPI stains nuclei. The upper row shows indicated single channels whereas overlays are shown in the bottom row. Negative controls for all secondary antibodies are shown in SI 4.

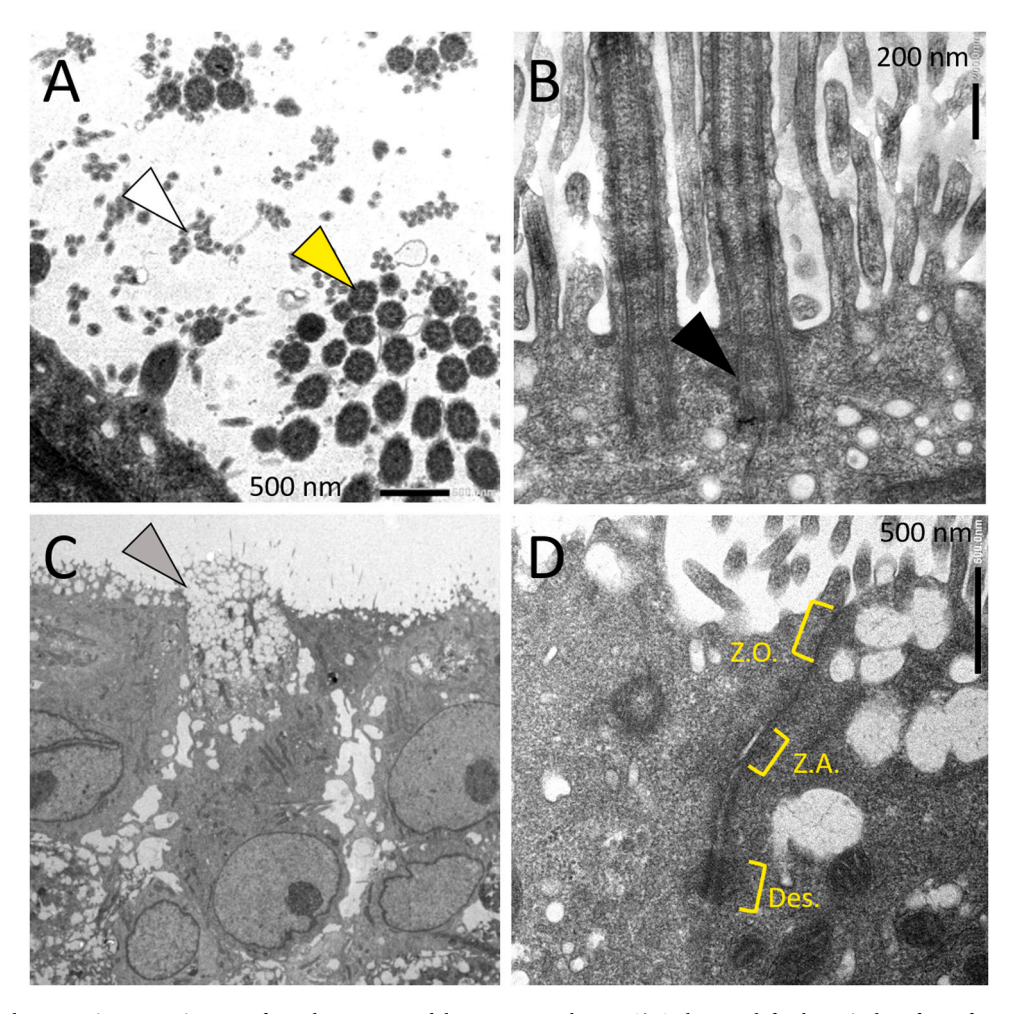


Fig. 2. Transmission electron microscopy images of nasal mucosa model on PET membrane. A) At bottom left, the apical surface of a model is visible. Round structures are sectioned kinocilia, in which the $9 \times 2 + 2$ microtubule structure can be seen (yellow arrowhead). Smaller structures are sectioned microvilli (white arrowhead). B) Kinocilium anchored in epithelial cell (black arrowhead) C) Goblet cell with protrusion towards the apical surface (grey arrowhead). D) Cell-cell contacts, such as zonula occludens (Z.O.)/tight junction, zonula adherens (Z.A.)/adherens junction and a desmosome are indicated. Examples from 3 donors are shown (B and C are from the same donor).

Data in Fig. 5 show no genotoxic effect. A consistent donor tendency for repair capacity can be suspected, as certain donors consistently exhibited low (donor 10, 2 h PE and donor 2 and 3, 24 h PE) or high (donor 6, 2 h and 24 h PE) % DNA tail values, including in the positive controls. Independent of CB, this pattern suggests donor variability in susceptibility to DNA damage and/or repair capacity.

3.5. Delayed epithelial barrier disruption

TEER measurements were performed at 2 h and 24 h PE to CB (Fig. 6). At 2 h PE, no differences were detected compared to the negative controls. Notably, at this timepoint, a slight increase in LDH release was observed at 4 µg/cm². The lack of a response in the TEER assay supports the interpretation that the LDH data (Fig. 4) does not indicate cytotoxicity. At 24 h PE, all conditions, including the negative control, showed lower TEER values compared to 2 h PE (Fig. 5). However, the values remained at levels strongly indicative of an intact barrier and epithelium. Donors included at both timepoints were donors 4, 6, 7, and 9. At $4 \,\mu\text{g/cm}^2$, the average TEER was lower than in the negative control (4 μ g/cm² = 500 Ohm*cm² vs. 723 Ohm*cm²; Welch's *t*-test p-value = 0.02). No significant difference was observed between 4 and $8 \mu g/cm^2$ exposures (p = 0.3). In addition, at 2 h PE where no disruption was indicated, a pronounced donor-specific trend was observed (Fig. 6A). In contrast, at 24 h PE, no such donor-specific pattern was evident. This discrepancy suggests that the lack of donorspecific behavior at 24 h PE reflects the influence of an external disturbance, in this case exposure to CB.

3.6. Inflammatory responses after particle exposure

Acute inflammatory responses 2 h PE were assessed by investigating the pro-inflammatory IL-6, IL-8, IL-1β, and TNFα, as well as the antiinflammatory IL-10. These cytokines were quantified in basal medium using a bead-antibody-based assay and flow cytometry. On average, no changes were seen in any cytokine in response to CB (Fig. 7). However, for individual cytokines, individual donors tended to display high or low values in all groups. Since this pattern for a given donor was not the same for all cytokines (e.g., not high for all measured cytokines, but only for specific ones) it cannot be ascribed to total higher concentrations due to, e.g., more cells present in certain donor models. Instead, this can be interpreted as a donor specific signature for each cytokine. As an example, donor 11 is among the lower expressing donors for all cytokines except TNFα, for which it expresses slightly more than other donors which were at the detection limit for this cytokine. Similarly, donor 14 was high for IL-6 and IL-8, but average for all other cytokines. At the individual donor level, one single donor displayed a trend in its response to increasing CB concentration, for IL-8, which decreased upon higher particle concentrations. This again highlights the importance of analyzing individual donors, and of including several donors in experiments.

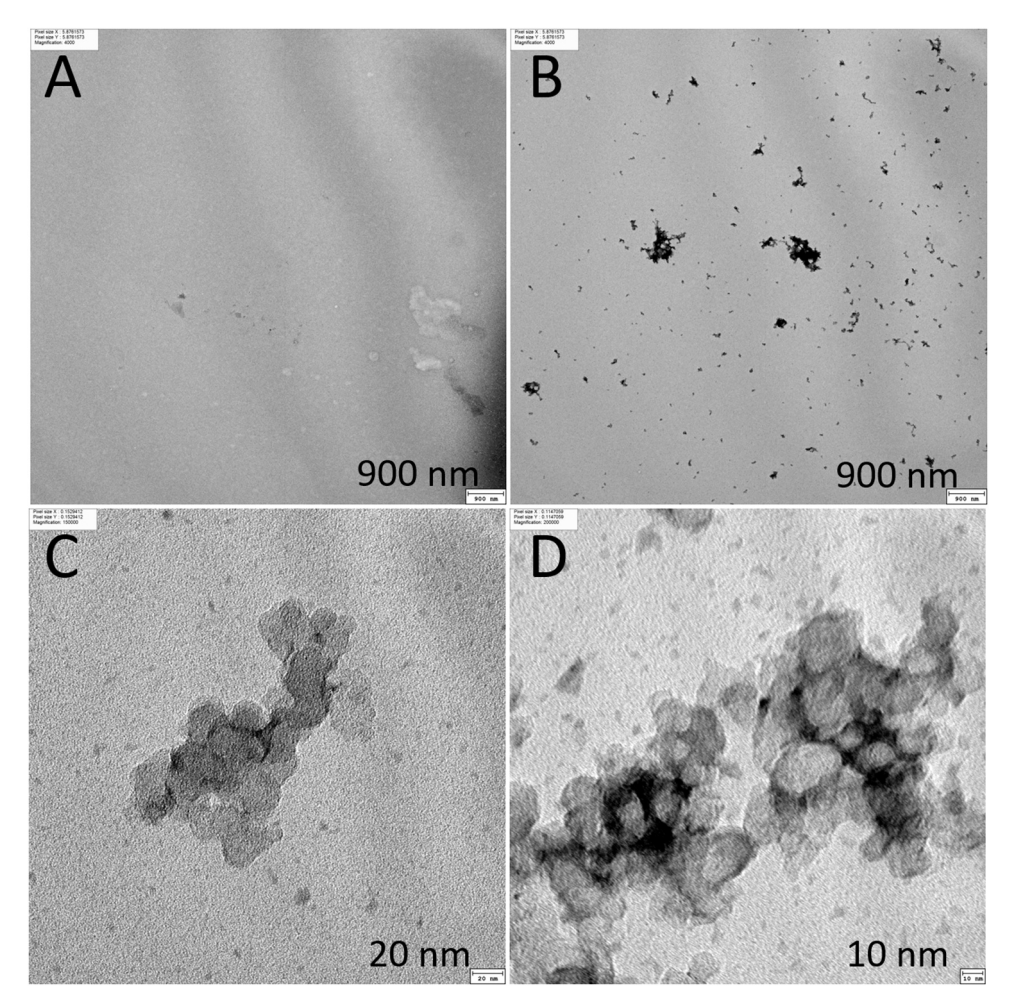


Fig. 3. CB prepared as for experiments in stock solution (2 μ g/ μ l). A) Negative control (only water), B-D) particles and particle agglomerates/aggregates at different magnifications. Primary particle diameters from approximately 15 nm and upwards to \sim 50 nm can be distinguished within particle agglomerates.

Table 2 Dynamic light scattering data of CB in double-distilled water and at different concentrations in cell culture medium (exposure medium). The concentrations were chosen so that they correspond to the resulting concentrations in $\mu g/cm^2$ on the cell inserts in the main experiments. PdI = polydispersity index. D(x) indicate intensity (i), volume (v) and particles numbers (n) percentiles for the 50th (0.5) percentiles, respectively. SI 5 shows particle number distributions.

Medium	Concentration [μg/ μl]	Corresponding concentration given for experiments $[\mu g/cm^2]$	Hydrodynamic diameter [nm]	PdI	D(i) 0.5	D(v) 0.5	D(n) 0.5
Double-distilled water Airway medium with 0,05 % BSA	0.30 0.003		$\begin{array}{c} 77\pm22\\128\pm56\end{array}$	0259 0189	125 186	127 238	73,3 110
Airway medium with 0,05 % BSA	0.03	1.0	92 ± 28	0134	156	184	88,8
Airway medium with 0,05 % BSA	0.13	4.0	102 ± 30	0124	146	157	97,6
Airway medium with 0,05 % BSA	0.29	8.0	116 ± 42	0131	180	229	106

3.7. TEM analysis reveals intracellular particles

Mucosa models exposed to CB and controls were prepared for TEM and imaged with the aim of 1) detecting particle-like structures, and 2) thoroughly assessing negative controls in the search of similar structures in order to determine whether they truly are CB or could be a result of assay artifacts. TEM is not a suitable method for quantification, but subjectively, no negative controls were found to contain particle-like structures. In contrast, samples exposed to high concentrations CB (4 and $8\,\mu\text{g/cm}^2)$ were investigated and found to contain comparable amounts of particle-like agglomerates (Fig. 8). Particles were found at

different intracellular localizations (Fig. 9) including the nucleus and did not appear to be encapsuled, $e.\ g.$, in lysosomes. Uncontrasted sections revealed the same type of structures (SI 6).

3.8. Donor overview

Using primary cells has scientific value and often improves the translational value of results. However, irregular cell numbers retrieved or differences in cell growth may limit the possibilities with regards to technical and biological replicates versus numbers of endpoints which can be applied. Here, in total 14 donors were included to complete the

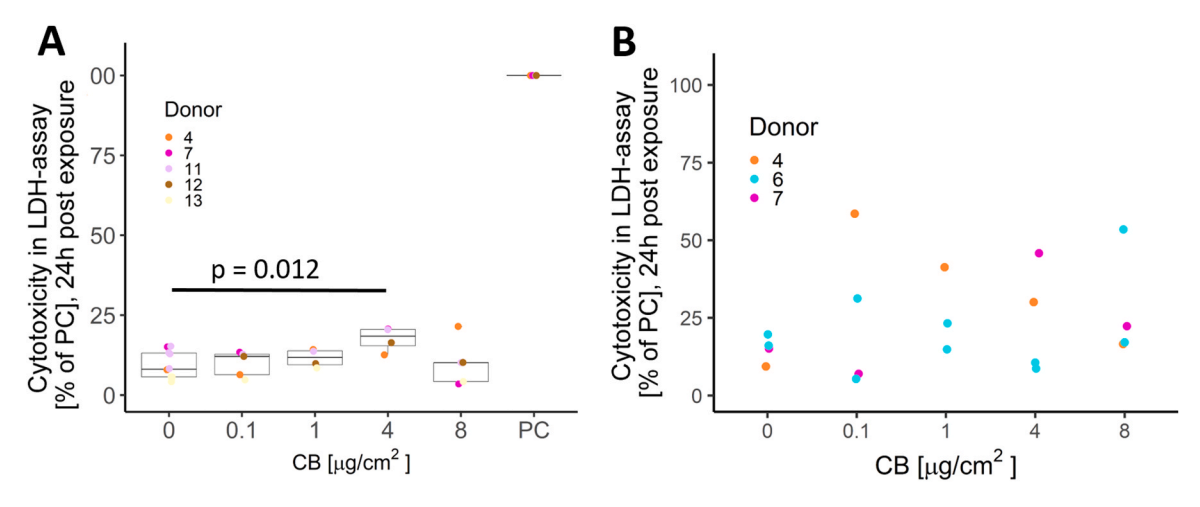


Fig. 4. LDH measurements from the apical wash, 2 h (A) and 24 h (B) post exposure (PE). A relatively high baseline in the negative control was observed, but no drastic increases were seen: comparing the LDH-release 2 h PE (A) between NC (absorbance (raw data) = 0.21, relative to PC = 9.3 %) with 4 μ g/cm² (absorbance = 0.43, relative to PC = 17.5 %) CB exposure suggests a mild effect at this concentration (Welch's *t*-test p-value = 0.012, n (donors = 5). At 8 μ g/cm² no difference from the NC was detected (mean = 9.9 %). 24 h PE (B), single measurements display higher LDH-values, some around 50 %, and a larger spread of datapoints can be seen. The low donor replicate number in B (n = 3) does not support statistical testing (or the use of boxplots).

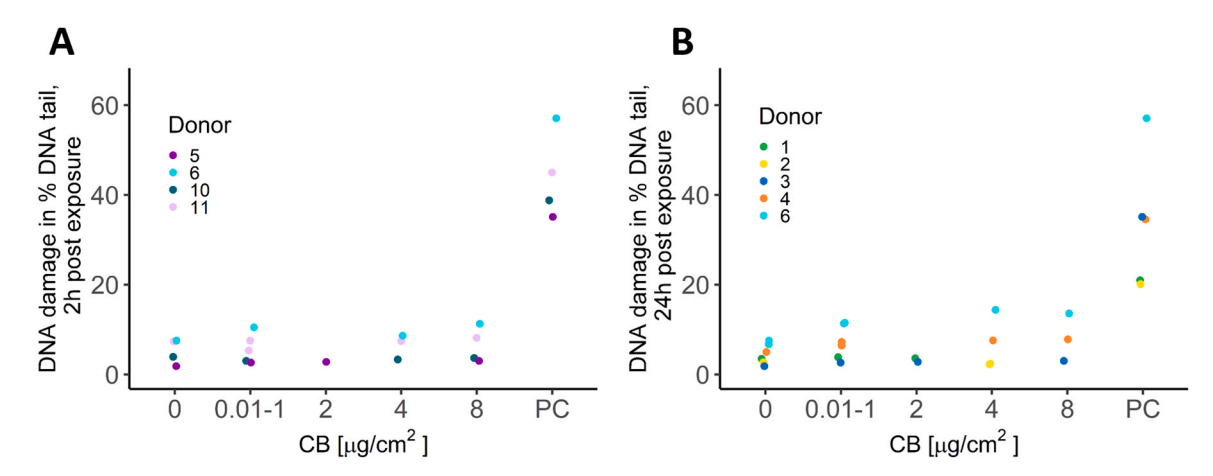


Fig. 5. Single cell gel electrophoresis (Comet assay) 2 h and 24 h post exposure (PE) at indicated concentrations. Positive controls (MMS, 2 h at 37° C and 5% CO₂) were included for all donors, consistently displaying higher % DNA tail than negative controls. With maximum 4 donors in each treated group (A and B), no statistical tests were performed. At 24 h (B), neither exposure of $0.01-1~\mu\text{g/cm}^2$ CB, nor $8~\mu\text{g/cm}^2$ were different from the negative control (mean = 7.2%; and = 8.1%, respectively, and the mean of the negative and positive controls were 4.5% and 33.6%, respectively). $n_{2,h}=4$, $n_{24,h}=5$.

different assays. Donor identities were indicated in all quantitative assays with a number (1-14) and a color for easier identification of donor patterns. In addition, an overview of how donor material was distributed in quantitative assays can be seen in Table 3.

4. Discussion

In vitro models of differentiated human upper respiratory mucosa were exposed to defined CB particles. The particles had a hydrodynamic average size of $\approx 77\,\mathrm{nm}$ diameter (DLS) and a primary particle size around 20 nm, as confirmed by TEM. Slightly larger sizes were detected when CB was dissolved in cell culture medium, a phenomenon previously reported for different types of media (Hussain et al., 2010; Pal et al., 2014). These particles can therefore serve as model particles for combustion-derived carbon ultrafine particles, for which existing experimental data is desired but scarce and challenging to generate. By establishing experimental approaches using simplified systems, necessary experiences and protocols were developed for more complex future exposures and measurements, e. g., using on-site generated and characterized UFP.

4.1. Intracellular particles detected

In this study, we qualitatively demonstrated that despite the presence of mucus and beating kinocilia, CB particles reach various localizations inside epithelial cells, including the nucleus and mitochondria. This evaluation was conducted using TEM, and control samples without contrasting agents (see SI 6) were analyzed to exclude the possibility of artifacts mimicking carbon particles. There were no notable tendencies for particle enrichment in specific localizations within the cell. Specifically, encapsulation in lysosomes, which has been described in the literature for several types of nanoparticles (Muntimadugu et al., 2022), was absent in our study. Notably, only particle agglomerates were observed, despite efforts to detect smaller fractions or granules. This preference for larger fractions is similar to the findings of Cronholm et al., who characterized < 400 nm sized copper nanoparticles (CuNP) used in exposure experiments (Cronholm et al., 2013). However, CuNP later found in cell nuclei were larger, mainly 0.5-1 µm in size. Although the authors could not determine whether particles had agglomerated/ aggregated before entering the nucleus or not, this may indicate a selectiveness for particle agglomerates for translocation to the cell nucleus. Our lack of specific particle localization suggests that cells do not

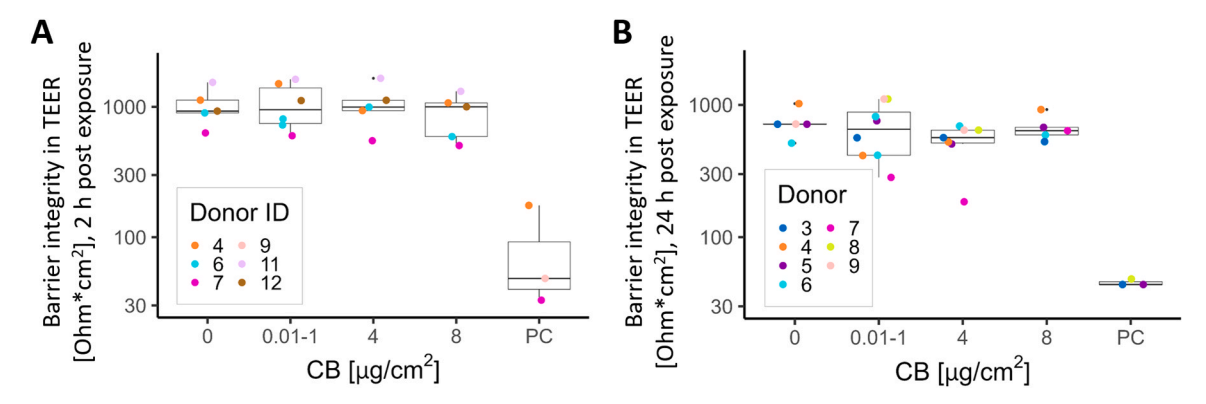


Fig. 6. Barrier integrity measurements by TEER, 2 h and 24 h post exposure (PE). Measurements from exposures in the concentration range $0.01-1 \,\mu\text{g/cm}^2$ have been merged for better visibility. At 2 h PE (A), the mean TEER of the negative control was $1024 \, \text{Ohm*cm}^2$. At 0.01-1, 4, and 8 $\mu\text{g/cm}^2$ the means were 1063, 1052, and 896 Ohm*cm^2 , respectively (Welch's *t*-test comparing $0.01-1 \,\mu\text{g/cm}^2$ to the NC resulted in p=0.87, comparing $8 \,\mu\text{g/cm}^2$ resulted in p=0.57; n=5). At $24 \, \text{h}$ PE (B), the mean TEER of the negative control was $737 \, \text{Ohm*cm}^2$. Means for 0.01-1, 4, and $8 \,\mu\text{g/cm}^2$ were 684, 537, and $672 \, \text{Ohm*cm}^2$, respectively (Welch's *t*-test comparing 0.01-1 to the negative control resulted in p=0.7, whereas comparing $4 \,\mu\text{g/cm}^2$ to the negative control gave p-value =0.09, n=4-8 for statistically tested concentrations). There was no difference between 4 and $8 \,\mu\text{g/cm}^2$ after $24 \, \text{h}$ (p=0.2). PC = 0.2 positive control (Staurosporin). At least two technical replicates (inserts) from each donor were analyzed in each experiment. Blanks (inserts with collagen coating only) were measured in each experiment, and was subtracted prior to any other analysis. Blank values were between 140 and 150 Ohm*cm^2 .

specifically detect the particles or recognize them as xenobiotics, or that protective responses are ineffective against this type of particle. However, the mild differences observed in toxicological and functional assays compared to negative controls indicate some level of tissue or cellular recognition of xenobiotics. Previous observations of the correlation between particle surface functionalization, such as by polycyclic hydrocarbons (PAHs), and the strength of cytotoxic effects (Lindner et al., 2017) suggest that our particles may have very low amounts of such toxic molecules on their surfaces. For instance, approximately 80 ng/g of US Environmental Protection Agency EPA priority PAH were detected in Printex 90 particles (Jacobsen et al., 2008). Furthermore, X-ray photoelectron spectroscopy surface composition analysis of Printex 90 carbon black particles revealed a predominantly carbon-based surface with minimal oxygen (0.5%) and sulfur (0.1%) and no detectable transition metals (Malmborg et al., 2025). The mild effects observed in this study may therefore result from a low but relevant presence of toxic surface molecules. Alternatively, in the absence of such surface molecules, weak effects caused by mechanical disruption may become detectable due to cellular uptake of agglomerates. A valuable future approach would be to use both "plain" and differently functionalized CB, similar to Lindner et al. in our differentiated human respiratory model. This would allow for a more detailed investigation of the respective roles of toxic molecules versus mechanical effects of particles in differentiated respiratory mucosa.

4.2. Barrier damage follows LDH-release at high doses of ultrafine CB

Two hours post exposure to CB, a mild increase in LDH release was measured in the apical compartment, which consists of differentiated respiratory epithelium. At this timepoint, no functional effects on barrier integrity were detected by TEER. Additionally, cytokine levels in the basal compartment showed no response to the selected cytokines. At 24 h PE, the barrier remained intact, with TEER values exceeding 300 Ohm*cm² for all conditions. However, a mild disturbance was observed at 24 h, as particle-exposed groups exhibited lower mean TEER values compared to negative controls. This mild barrier disturbance - but a still intact barrier - supports the hypothesis that the LDH release at 2 h PE resulted from membrane damage rather than cell death, with membrane integrity likely restored by 24 h PE. Membrane repair is a fast process and its mechanism depends on the extent of the damage. Small (nanometer-scale) wounds are repaired through the lateral flow of lipids, while larger wounds require a Ca²⁺- and exocytosis-dependent mechanism (Cong et al., 2017). The 24 h PE decrease in barrier function could be a consequence of such hypothesized membrane damage and repair. Reduced electrical resistance over the epithelial barrier indicates that tight junctions have been disrupted and become more permeable. Changes in tight junction functionality can be linked to membrane-bound proteins such as ion channels and nutrient transporters (Liang and Weber, 2014) and tight junction proteins interact with the cytoskeleton (Turner et al., 1997). On the one hand, tight junctions appear to be maintained during epithelial renewal and physiological or pathological shedding of cells, a process which involves cell polarity changes and controlled re-localization of tight junction proteins (Marchiando et al., 2011). Similarly, polarity is used in healthy cells to separate molecules (apical/basal separation) which, when they interact induce repair mechanisms, a cascade which becomes initiated upon, e.g., membrane damage (Vermeer et al., 2003). This process also appears to involve tight junction proteins and changes in barrier functionality. These described crosstalk mechanisms between the apical plasma membrane (and damage thereof) and the epithelial barrier and tight junctions suggest, that apical LDH leakage followed by barrier disturbance could be mechanistically linked processes. Follow-up studies which monitor membrane damage, specific membrane bound proteins, TEER and tight junctional protein localization over time post CB or other UFP exposure would be informative to investigate such hypotheses. It can however not be excluded that the two observations are mechanistically separated events in response to CB exposure. Long-term observations post exposure, inclusion of more timepoints, and repeated exposures will be important to better understand whether the subtle changes described here may be physiologically relevant and whether they are mechanistically linked or not.

Other studies have variably reported cytotoxicity following CB exposure in respiratory *in vitro* models, including alveolar models (Hussain et al., 2010; Niranjan and Thakur, 2017). Some studies found no cytotoxic effects or observed effects only at an extreme concentration (Chaudhuri et al., 2018; Niranjan and Thakur, 2017; Di Ianni et al., 2021). One proposed reason for such differences is that the surface chemistry of nanoparticles and UFP is relevant for toxicological responses (Lindner et al., 2017; Al Housseiny et al., 2020). Surface manipulation of PAHs on CB influenced the cytotoxic effects of particles in a study showing that CB without active addition of PAH had the least cytotoxic effects in cell lines and in rodent experiments (Lindner et al., 2017). Similar results, with and without addition of defined hydrocarbons, have later been reported for black carbon, a carbon particle component of incomplete combustion, on an alveolar cell line (A549) in co-culture with monocytes (THP-1) (Hakkarainen et al., 2022). Taken

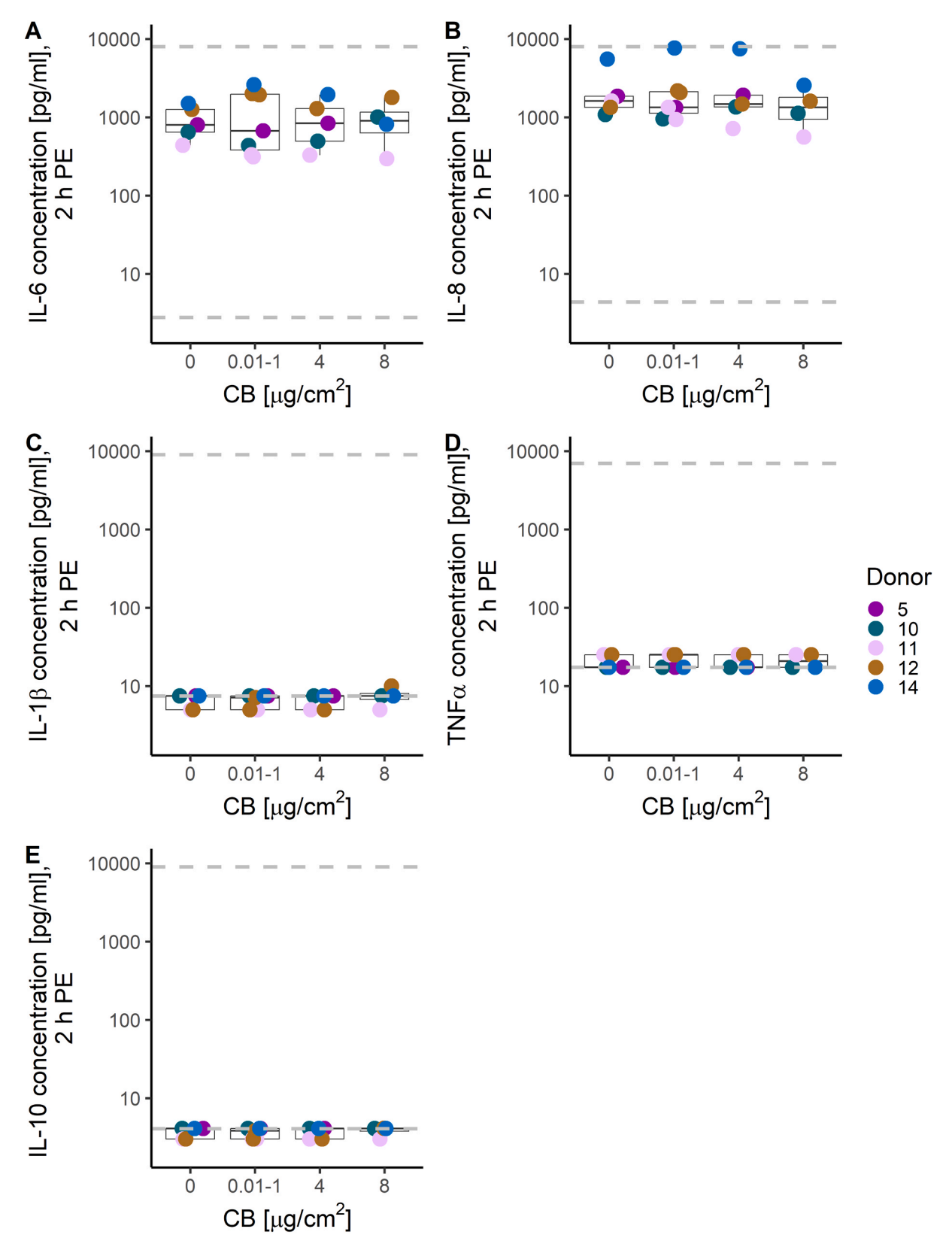


Fig. 7. Basally released IL-6, IL-1 β , TNF α , and IL-10 were quantified 2 h PE using a bead-antibody assay and detection by flow cytometry. The individual cytokines are indicated in plots A to E with dashed grey lines indicating upper and lower detection limits. On average, no change upon particle exposure was detected. Individual donors stand out and suggest weak concentration dependent responses for IL-8 (donor 14 decreasing from high value, donor 11 decreasing from low value). Detection limits in pg/ml for the respective cytokines were: IL-6 = 2.8; IL-8 = 4.4; IL-1 β = 7.5, TNF α = 17.4; and IL-10 = 4.1. Upper quantification limits in pg/µl for cytokines were: IL-6 and IL-8 = 8000; IL-1 β and IL-10 = 9000; and TNF α = 7000. Given the minimal changes in averages, no statistical testing was motivated.

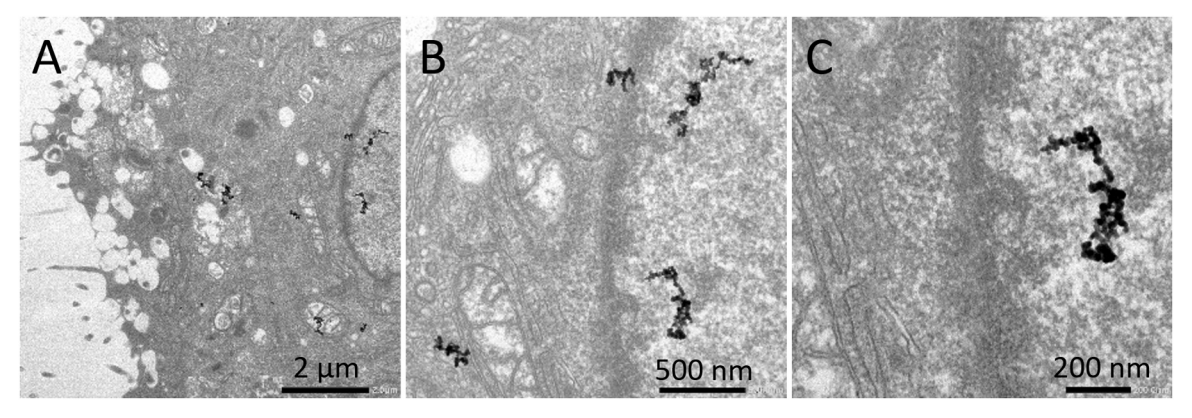


Fig. 8. Intracellular particles/particle agglomerates were detected at the concentrations applied in the current study (here examples from $8 \mu g/cm^2$ in donor 12, 2 h PE). The example shows suspected particles in the cytoplasm (A) as well as in the nucleus of one cell (B and C). The lack of similar particle-like structures in uncontrasted sections (SI 6), in the extracellular space, and the uneven distribution in the entire model speak against these particles being contrasting artifacts.

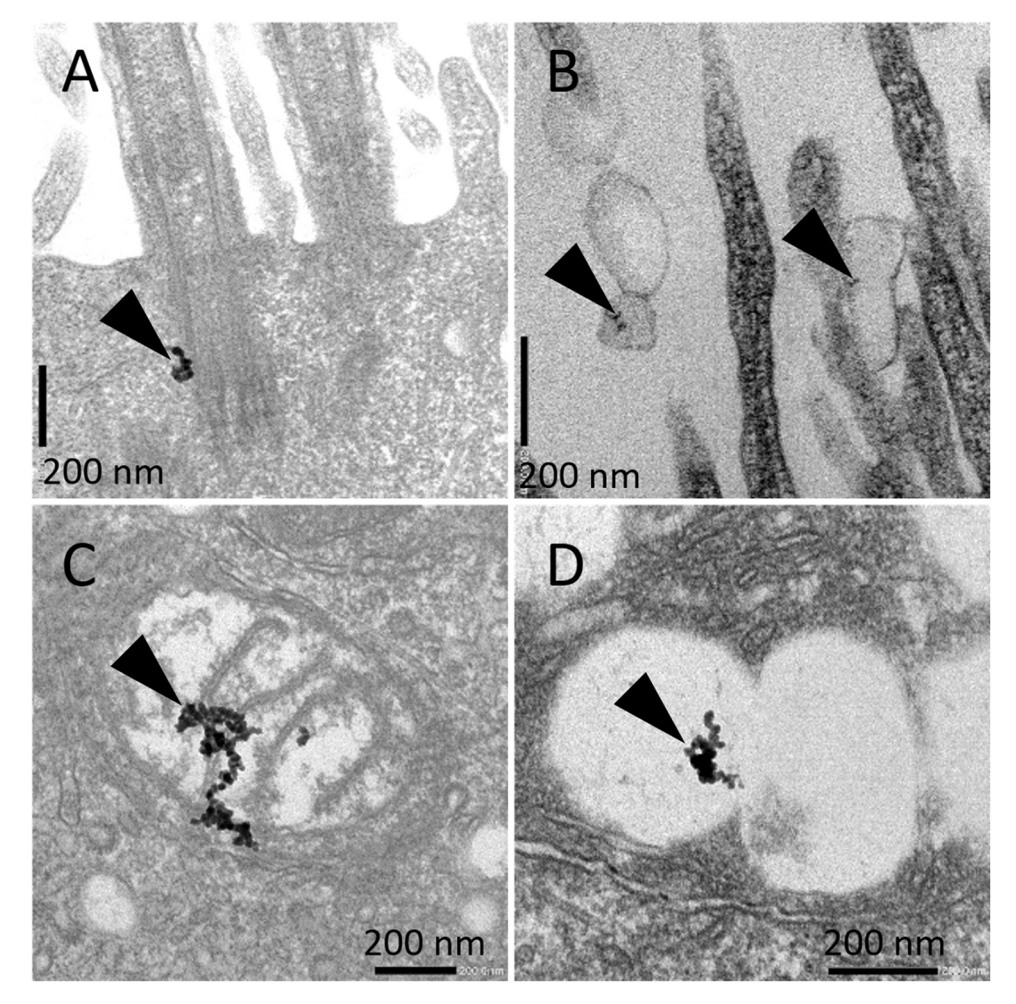


Fig. 9. Intracellular particles were found at varying intracellular localizations but did not appear to localize to specific organelles or structures. Particles were only rarely seen extracellularly, and when, in association with kinocilia or vesicles. Particles indicated by black arrows at A) base of a kinocilium, B) extracellular vesicle, C) mitochondrion, and D) vesicle, possibly mucus-filled, based on similarity with such vesicles in goblet cells.

together, those studies suggest that potential toxic or otherwise harmful effects of CB likely act via surface-functionalization which in turn regulates the intrinsic oxidative potential of carbon black particles. Notably, it was recently shown that reactive oxygen species production increases with carbon sp2-hybridization and sulfur oxide surface content (Malmborg et al., 2025).

4.3. No alteration of inflammatory markers after CB exposure

No effects of CB were seen on the release of selected inflammation markers (IL-1 β , IL-6, IL-8, IL-10 and TNF α) 2 h post exposure. Accumulated IL-6 and IL-8 were present at > 1000 pg/ml medium, with some donor samples for IL-8 at the upper quantification limit of 9000 pg/ml. High levels of these two cytokines are expected for the respiratory

Table 3Detailed listing of donor usage in different quantitative assays. If the donor was only available for analysis in one of the two timepoints, the used timepoint is indicated in the column "Assays".

Donor number	Donor represented in # assays	Assays
1	3	LDH, Comet (24 h), TEER
2	1	Comet (24 h)
3	2	Comet (24 h), TEER (24 h)
4	3	LDH, Comet (24 h), TEER
5	3	Comet (2 h), TEER (24 h), Cytokines
6	3	LDH (24 h), Comet, TEER
7	2	LDH and TEER
8	1	TEER (24 h)
9	1	TEER
10	2	Comet (2 h), Cytokines
11	3	LDH (2 h), Comet (2 h), TEER, (2 h),
		Cytokines
12	2	LDH (2 h), TEER (2 h), Cytokines
13	1	LDH (2 h)
14	1	Cytokines

epithelium (Becker et al., 1993; Gras et al., 2010), serving as confirmation that the models accurately reflect aspects of the innate immune defense in this niche. In contrast, IL-1 β , IL-10, and TNF α were either not detected in all samples or were detected at low levels. However, differences between donors were still observed even in the lower ranges for these three cytokines. Two donors (11 and 12) displayed lower levels of IL-1 β and IL-10, whereas they were higher than the other four donors for TNFα. Donor 14 showed a tendency for a concentration-dependent response for IL-6, and for IL-8; a difference was seen only at the highest concentration CB. Similarly, Donor 11 appeared to respond with a concentration-dependent reduction in IL-8 only. Other donors differed from one-another (high/intermediate/low) without showing signs of response to CB. Statistical differences for the investigated group of donors were not detected. Although changes or trends seen in single donors must be carefully interpreted, one may speculate that these donors represent different responder categories in the human population (e.g. high, low, intermediate). However, to test this hypothesis, an estimated 5–10-fold higher number of donors should be used in the assays applied in this study to enable detection of statistically significant differences with a high number of responder types. Alternatively, donor subgroups could be identified beforehand and selected for targeted experiments. That approach is not possible with the donor data available in this study. Accessing such meta-data on donors would require additional ethical consideration and approval. Other possible reasons for the absence of statistically significant differences are, apart from an actual true lack of a response, 1) a different selection of cytokines to analyze, 2) the lack of some systemic/immune related factor in the model, which is necessary to induce a response, 3) changes are not detectable at the timepoints used in this study, 4) the cytokines are not secreted (supernatants were investigated). Theoretically, a more complex model which includes selected immune cells is a possible solution to the second explanation model, although choosing the molecule or cell type to add is not trivial. In the case of cells, establishment of such cell systems with, e.g., suitable media for all cell types is a challenging task. Alternatively, 5) the exposure setup is suboptimal to detect changes in cytokines. Example parameters are duration of each exposure or repeated exposures (in which also duration, delay times and number of repetitions become parameters). The wide range of possibilities in our opinion demonstrates that this research can be carried out with different approaches: multiparameter approaches in which assays, donors and exposure settings are varied (very complex, resource (and donor) demanding, and possibly difficult to interpret), or in experiments of lower complexity which could focus on effects of, e.g., exposure settings (as exemplified above) or comprehensive analysis of biological responses (different assays) or donor variability, keeping other parameters constant and at low

complexity. The latter is for most research labs the more realistic approach and will contribute to narrowing down the complexity in future multiparameter experiments.

4.4. Considerations for particle-cell interactions and the importance of model choice

It has been observed that ciliary beat frequency in the respiratory epithelium of ex vivo mouse trachea increases upon exposure to higher CB concentrations, which also coincided with increased particle agglomeration at higher concentrations. In that study, particle transport speed was influenced by the amount of mucus (Lindner et al., 2017). However, Roth et al. noted differences in the structure and function of mucociliary clearance between human and rats (Roth et al., 2025). This raises questions about the validity of animal models such as the mouse in Lindner et al. to model mucociliary clearance in humans (Roth et al., 2025). Additionally, human cell line-based models of the respiratory epithelium have limitations when it comes to simulating mucociliary differentiation and function. For instance, ALI-cultured Calu-3 cells lack kinocilia (Lodes et al., 2020), which are crucial for mucociliary clearance. Using models with a higher in vitro - in vivo correlation could potentially yield different, more accurate results. Ciliary beat frequency may also serve an additional purpose beyond transporting mucus (and particles) laterally, such as keeping particles in the mucus solution and hindering them from attaching to or entering cells. In addition, the composition of mucins, DNA, other small molecules, and water in mucus may also influence particle behavior via, e.g., corresponding changes in the mucus' viscoelastic properties. Particle translocation is influenced by parameters such as temperature and fluid viscosity. Generally, very small particles (<10 nm) mainly move by diffusion, while relatively large (>200 nm) and dense particles are transported primarily by sedimentation, which could apply to UFP or nanoparticle agglomerates, respectively. Both of these small and large categories tend to be transported quickly, whereas the majority of intermediate sized nanoparticles (10 – 100 nm) move at a slower pace. This could increase the possibility for uptake of this particle category since they may have more time to interact with cells. Furthermore, our study aimed to address functional effects of inhaled particles, with particular focus on barrier functionality. Epidemiological data does not indicate extensive acute cytotoxicity following PM-exposure but instead points to long-term effects of inhaled pollutants. A potential mechanistic explanation for these long-term effects could be repeated mild disruptions to the epithelial barrier, which may occasionally allow otherwise harmless pathogens or particles to penetrate deeper tissues in the upper airways or even enter the systemic circulation. Our data supports this direction, showing no strong, acute effects in mucosa models, apart from barely detectable acute LDH leakage and a mild reduction in barrier integrity 24 h after exposure. Continued work on improving in vitro models for repeated exposures and long-term studies will enhance our ability to experimentally address such hypotheses, with the aim of providing better evidence for risk assessment, and protective and realistic particle limit values for every-day life.

4.5. Relevance of this study for future research and risk assessment

The overall aim of this and the authors' related research is to provide more reliable data for risk assessment for ultrafine particles by improving existing targeted *in vitro* models and exposure setups – *i.e.* including exposure conditions and particle handling. This study established an experimental exposure setup at the ALI with model UFP for a complex mucosal respiratory model. Using high concentrations of model UFP, first insights into response mechanisms were gained. The concentrations applied here, re-calculated to $\rm m^3$, were ~ 3 orders of magnitude higher than, *e.g.*, EU limit values for $\rm PM_{2.5}$ or $\rm PM_{10}$ (50 $\rm \mu g/m^3$) in ambient air (Directive 2008/50/EC; for UFP limits have not yet been defined). Those limits compare in size with measured values on, for

instance, a construction site (peak value 44 µg/m³, (Ferree et al., 2024) or similarly, an average 47 μ g/m³ organic carbon and ~78 μ g/m³ total carbon in an underground excavation site (Park et al., 2020). Breathing in one breath, approximately ~ 0.5 l, of such air would correspond to 0.225 µg particles. Assuming 15 breaths per minute, breathing such air for slightly more than 3 h would correspond to 4 μg/cm² or for just over 6 h to 8 μg/cm² (again assuming full deposition. See all assumptions and calculations in SI 7). Although this simplified calculation makes some assumptions that may be discussed, the numbers suggest that a person could be exposed to concentrations similar to those used in our study within a number of days on a highly exposed workplace. This does not enable 1:1 comparisons with real-life and does not include the interaction between UFPs and other compounds present in ambient air (e.g., microplastics, pollen, pathogens). Nevertheless, it suggests that the readouts from the models may have in vivo relevance and that including the concentrations used as the maximum of the concentration range in future studies could be informative.

This study also contributes to methodological development. Establishing new methodologies involves the necessity to confirm the use of proper endpoints/assays, identify potential artifacts, confirm the detection of desired readouts (e.g. particles visible by TEM). In addition, this work enabled the authors to initialize work to narrow down the number of endpoints and address more specific hypotheses in future studies. A benefit of this approach is that it becomes realistic to include more timepoints and/or more donors. The practically highest possible exposure concentration in our setting was included with the aim to increase the chance for interpretable readouts within the used setting. The authors consider it important to transparently report also lack of responses to the research community. In this context, this study is highly relevant as a further step towards more realistic in vitro exposures. Considering the indications here for a disturbed barrier and membrane damage upon UFP exposure, it is promising to continue the research using such mucosal in vitro models for repeated exposures and long-term studies in order to identify potential long-term effects of UFP exposure.

Funding

This work was funded by the Bavarian State Ministry of the Environment and Consumer Protection. The transmission electron microscope JEOL JEM-1400 FLash is funded by the Deutsche Forschungsgemeinschaft (DFG, German Research Foundation) – 426173797 (INST 93/1003–1 FUGG) the JEOL JEM 2100 by the same institution under the funding number 218894895.

CRediT authorship contribution statement

Stephan Hackenberg: Writing – review & editing, Supervision, Project administration, Funding acquisition, Conceptualization. Totta Ehret Kasemo: Writing – review & editing, Writing – original draft, Visualization, Project administration, Formal analysis, Data curation, Conceptualization. Meyer Till Jasper: Writing – review & editing, Supervision, Project administration, Funding acquisition, Conceptualization. Maximilian Oppmann: Writing – review & editing, Visualization. Maximilian Oppmann: Writing – review & editing, Visualization, Formal analysis, Data curation, Conceptualization. Ralf Zimmermann: Supervision. Sebastiano Di Bucchianico: Writing – review & editing. Elena Lajtha: Data curation. Helena Moratin: Writing – review & editing. Sofia Dembski: Writing – review & editing, Conceptualization. Maria Steinke: Writing – review & editing. Manuel Stöth: Writing – review & editing, Supervision, Funding acquisition, Conceptualization. Mathilde Noémie Delaval: Writing – review & editing.

Declaration of Competing Interest

The authors declare the following financial interests/personal relationships which may be considered as potential competing interests: Till Jasper Meyer reports financial support was provided by Bavarian State Ministry of the Environment and Consumer Protection. If there are other authors, they declare that they have no known competing financial interests or personal relationships that could have appeared to influence the work reported in this paper.

Acknowledgements

The authors thank Christian Stigloher, Daniela Bunsen, and Claudia Gehrig-Höhn (University of Würzburg, Imaging Core Facility at the Theodor-Boveri-Institute of Bioscience) for their extensive support with TEM analysis (instrument funded by the German Research Foundation DFG, 426173797 (INST 93/1003–1 FUGG)) and JEOL JEM-2100 (funding 218894163). We thank Corinna Geßner, Laura Halbhuber, Silke Hummel, Barbara Kellner, Michael Kessler, Heike Oberwinkler, and Maria Scheurich (University Hospital Würzburg, Department of Oto-Rhino-Laryngology, Head and Neck Surgery) for their excellent technical assistance and support.

Appendix A. Supporting information

Supplementary data associated with this article can be found in the online version at doi:10.1016/j.etap.2025.104829.

Data availability

Data will be made available on request.

References

- Adcock, I., Novotny, T., Nic, M., Dibusz, K., Hynes, J., Marshall, L., Gribaldo, L., 2020.
 Advanced non-animal models in biomedical research. Respiratory tract diseases.
 Publications Office of the European Union.
- Aghapour, M., Raee, P., Moghaddam, S.J., Hiemstra, P.S., Heijink, I.H., 2018. Airway epithelial barrier dysfunction in chronic obstructive pulmonary disease: role of cigarette smoke exposure. Am. J. Respir. Cell Mol. Biol. 58 (2), 157–169.
- Al Housseiny, H., Singh, M., Emile, S., Nicoleau, M., Wal, R.L.V., Silveyra, P., 2020. Identification of toxicity parameters associated with combustion produced soot surface chemistry and particle structure by in vitro assays. Biomedicines 8 (9).
- Becker, S., Koren, H.S., Henke, D.C., 1993. Interleukin-8 expression in normal nasal epithelium and its modulation by infection with respiratory syncytial virus and cytokines tumor necrosis factor, interleukin-1, and interleukin-6. Am. J. Respir. Cell Mol. Biol. 8 (1), 20–27.
- Boland, S., Baeza-Squiban, A., Fournier, T., Houcine, O., Gendron, M.C., Chévrier, M., Jouvenot, G., Coste, A., Aubier, M., Marano, F., 1999. Diesel exhaust particles are taken up by human airway epithelial cells in vitro and alter cytokine production. Am. J. Physiol. 276 (4), L604–613.
- Boraschi, D. Validated protocols for test item preparation for key in vitro and ecotoxicity studies. NANoREG deliverable D 2.06 (2017). Nederlands National Institute for Public Health and the Environment.
- Borisova, T., Komisarenko, S., 2021. Air pollution particulate matter as a potential carrier of SARS-CoV-2 to the nervous system and/or neurological symptom enhancer: arguments in favor. Environ. Sci. Pollut. Res. 28 (30), 40371–40377.
- Chalvatzaki, E., Chatoutsidou, S.E., Diapouli, L., Gini, M.I., Manousakas, M.I., Samoli, E., Eleftheriadis, K., Lazaridis, M., 2025. Dosimetry simulations of ultrafine particles deposition to the human respiratory tract and transport to the olfactory region for female receptors. Atmos. Environ. 348.
- Chaudhuri, I., Fruijtier-Pölloth, C., Ngiewih, Y., Levy, L., 2018. Evaluating the evidence on genotoxicity and reproductive toxicity of carbon black: a critical review. Crit. Rev. Toxicol. 48 (2), 143–169.
- Comer, D.M., Elborn, J.S., Ennis, M., 2012. Comparison of nasal and bronchial epithelial cells obtained from patients with COPD. PLoS One 7 (3), e32924.
- Cong, X., Hubmayr, R.D., Li, C., Zhao, X., 2017. Plasma membrane wounding and repair in pulmonary diseases. Am. J. Physiol. Lung Cell Mol. Physiol. 312 (3), L371–l391.
- Cronholm, P., Karlsson, H.L., Hedberg, J., Lowe, T.A., Winnberg, L., Elihn, K., Wallinder, I.O., Möller, L., 2013. Intracellular uptake and toxicity of ag and CuO nanoparticles: a comparison between nanoparticles and their corresponding metal ions. Small 9 (7), 970–982.
- Deprez, M., Zaragosi, L.E., Truchi, M., Becavin, C., Ruiz Garcia, S., Arguel, M.J., Plaisant, M., Magnone, V., Lebrigand, K., Abelanet, S., Brau, F., Paquet, A., Pe'er, D., Marquette, C.H., Leroy, S., Barbry, P., 2020. A Single-Cell Atlas of the human healthy airways. Am. J. Respir. Crit. Care Med 202 (12), 1636–1645.
- Di Ianni, E., Erdem, J.S., Moller, P., Sahlgren, N.M., Poulsen, S.S., Knudsen, K.B., Zienolddiny, S., Saber, A.T., Wallin, H., Vogel, U., Jacobsen, N.R., 2021. In vitro-in vivo correlations of pulmonary inflammogenicity and genotoxicity of MWCNT. Part Fibre Toxicol. 18 (1), 25.

- Di Ianni, E., Jacobsen, N.R., Vogel, U.B., Moller, P., 2022. Systematic review on primary and secondary genotoxicity of carbon black nanoparticles in mammalian cells and animals. Mutat. Res Rev. Mutat. Res 790, 108441.
- Ding, Y., Weindl, P., Lenz, A.G., Mayer, P., Krebs, T., Schmid, O., 2020. Quartz crystal microbalances (QCM) are suitable for real-time dosimetry in nanotoxicological studies using VITROCELL®Cloud cell exposure systems. Part Fibre Toxicol. 17 (1), 44.
- Facciola, A., Visalli, G., La Maestra, S., Ceccarelli, M., Aleo, F.D., Nunnari, G., Pellicano, G.F., Di Pietro, A., 2019. Carbon nanotubes and central nervous system: environmental risks, toxicological aspects and future perspectives. Environ. Toxicol. Pharm. 65, 23–30.
- Ferree, P.L., Polat, M., Nojgaard, J.K., Jensen, K.A., 2024. Airborne particulate matter and diesel engine exhaust on infrastructure construction sites in the Copenhagen metropolitan area. Ann. Work Expo. Health 68 (8), 791–803.
- Gizurarson, S., 2012. Anatomical and histological factors affecting intranasal drug and vaccine delivery. Curr. Drug Deliv. 9, 566–582.
- Gras, D., Tiers, L., Vachier, I., de Senneville, L.D., Bourdin, A., Godard, P., Lehman, S., Chanez, P., 2010. Regulation of CXCR/IL-8 in human airway epithelial cells. Int Arch. Allergy Immunol. 152 (2), 140–150.
- Hakkarainen, H., Salo, L., Mikkonen, S., Saarikoski, S., Aurela, M., Teinilä, K., Ihalainen, M., Martikainen, S., Marjanen, P., Lepistö, T., Kuittinen, N., Saamio, K., Aakko-Saksa, P., Pfeiffer, T.V., Timonen, H., Rönkkö, T., Jalava, P.I., 2022. Black carbon toxicity dependence on particle coating: measurements with a novel cell exposure method. Sci. Total Environ. 838 (Pt 4), 156543.
- Hiemstra, P.S., Grootaers, G., van der Does, A.M., Krul, C.A.M., Kooter, I.M., 2018. Human lung epithelial cell cultures for analysis of inhaled toxicants: lessons learned and future directions. Toxicol. Vitr. 47, 137–146.
- Hussain, S., Thomassen, L.C., Ferecatu, I., Borot, M.C., Andreau, K., Martens, J.A., Fleury, J., Baeza-Squiban, A., Marano, F., Boland, S., 2010. Carbon black and titanium dioxide nanoparticles elicit distinct apoptotic pathways in bronchial epithelial cells. Part Fibre Toxicol. 7, 10.
- Jaber, N., Billet, S., 2024. How to use an in vitro approach to characterize the toxicity of airborne compounds. Toxicol. Vitr. 94, 105718.
- Jacobsen, N.R., Pojana, G., White, P., Møller, P., Cohn, C.A., Korsholm, K.S., Vogel, U., Marcomini, A., Loft, S., Wallin, H., 2008. Genotoxicity, cytotoxicity, and reactive oxygen species induced by single-walled carbon nanotubes and C(60) fullerenes in the FE1-Mutatrade markmouse lung epithelial cells. Environ. Mol. Mutagen 49 (6), 476–487.
- Kelly, J.T., Asgharian, B., Kimbell, J.S., Wong, B.A., 2004. Particle deposition in human nasal airway replicas manufactured by different methods. Part II: ultrafine particles. Aerosol Sci. Technol. 38 (11), 1072–1079.
- Lacroix, G., Koch, W., Ritter, D., Gutleb, A.C., Larsen, S.T., Loret, T., Zanetti, F., Constant, S., Chortarea, S., Rothen-Rutishauser, B., Hiemstra, P.S., Frejafon, E., Hubert, P., Gribaldo, L., Kearns, P., Aublant, J.M., Diabaté, S., Weiss, C., de Groot, A., Kooter, I., 2018. Air-Liquid interface in vitro models for respiratory toxicology research: consensus workshop and recommendations. Appl. Vitr. Toxicol. 4 (2), 91–106.
- Lehmann, J.S., Rughwani, P., Kolenovic, M., Ji, S., Sun, B., 2019. LEGENDplex™: Beadassisted multiplex cytokine profiling by flow cytometry. Methods Enzym. 629, 151–176.
- Leikauf, G.D., Kim, S.H., Jang, A.S., 2020. Mechanisms of ultrafine particle-induced respiratory health effects. Exp. Mol. Med 52 (3), 329–337.
- Leopold, D.A., 1992. Pollution: the nose and sinuses. Otolaryngol. Head. Neck Surg. 106 (6), 713–719.
- Liang, G.H., Weber, C.R., 2014. Molecular aspects of tight junction barrier function. Curr. Opin. Pharm. 19, 84–89.
- Lindner, K., Ströbele, M., Schlick, S., Webering, S., Jenckel, A., Kopf, J., Danov, O.,
 Sewald, K., Buj, C., Creutzenberg, O., Tillmann, T., Pohlmann, G., Ernst, H.,
 Ziemann, C., Hüttmann, G., Heine, H., Bockhorn, H., Hansen, T., König, P.,
 Fehrenbach, H., 2017. Biological effects of carbon black nanoparticles are changed
 by surface coating with polycyclic aromatic hydrocarbons. Part Fibre Toxicol. 14 (1),
 8.
- Lindner, K., Ströbele, M., Schlick, S., Webering, S., Jenckel, A., Kopf, J., Danov, O., Sewald, K., Buj, C., Creutzenberg, O., Tillmann, T., Pohlmann, G., Ernst, H., Ziemann, C., Hüttmann, G., Heine, H., Bockhorn, H., Hansen, T., König, P., Fehrenbach, H., 2017. Biological effects of carbon black nanoparticles are changed by surface coating with polycyclic aromatic hydrocarbons. Part. Fibre Toxicol. 14 (1), 1–17.
- Lodes, N., Seidensticker, K., Perniss, A., Nietzer, S., Oberwinkler, H., May, T., Walles, T., Hebestreit, H., Hackenberg, S., Steinke, M., 2020. Investigation on ciliary functionality of different airway epithelial cell lines in Three-Dimensional cell culture. Tissue Eng. Part A 26 (7-8), 432–440.
- Malmborg, V., Elam, D.A., Di Battista, V., Rissler, J., Clausen, P.A., Vogel, U., Wohlleben, W., Jacobsen, N.R., 2025. Toxicity of carbon nanomaterials: a model to predict ROS production from easily measurable surface characteristics. Carbon 234, 119997.
- Mao, S., Shah, A.S., Moninger, T.O., Ostedgaard, L.S., Lu, L., Tang, X.X., Thornell, I.M., Reznikov, L.R., Ernst, S.E., Karp, P.H., Tan, P., Keshavjee, S., Abou Alaiwa, M.H., Welsh, M.J., 2018. Motile cilia of human airway epithelia contain hedgehog signaling components that mediate noncanonical hedgehog signaling. Proc. Natl. Acad. Sci. USA 115 (6), 1370–1375.
- Marchiando, A.M., Shen, L., Graham, W.V., Edelblum, K.L., Duckworth, C.A., Guan, Y., Montrose, M.H., Turner, J.R., Watson, A.J., 2011. The epithelial barrier is maintained by in vivo tight junction expansion during pathologic intestinal epithelial shedding. Gastroenterology 140 (4), 1208–1218 e1201–1202.

- Meyer, T.J., Tekin, N., Hense, P., Ehret-Kasemo, T., Lodes, N., Stöth, M., Ickrath, P., Gehrke, T., Hagen, R., Dembski, S., Peer, M., Steinke, M.R., Scherzad, A., Hackenberg, S., 2023. Evaluation of the cytotoxic and genotoxic potential of printer toner particles in a 3D air-liquid interface, primary cell-based nasal tissue model. Toxicol. Lett.
- Muntimadugu, E., Silva-Abreu, M., Vives, G., Loeck, M., Pham, V., Del Moral, M., Solomon, M., Muro, S., 2022. Comparison between nanoparticle encapsulation and surface loading for lysosomal enzyme replacement therapy. Int. J. Mol. Sci. 23 (7).
- Niranjan, R., Thakur, A.K., 2017. The toxicological mechanisms of environmental soot (Black Carbon) and carbon black: focus on oxidative stress and inflammatory pathways. Front. Immunol. 8, 763.
- Ohlwein, S., Kappeler, R., Kutlar Joss, M., Künzli, N., Hoffmann, B., 2019. Health effects of ultrafine particles: a systematic literature review update of epidemiological evidence. Int. J. Public Health 64 (4), 547–559.
- Pal, A.K., Aalaei, I., Gadde, S., Gaines, P., Schmidt, D., Demokritou, P., Bello, D., 2014. High resolution characterization of engineered nanomaterial dispersions in complex media using tunable resistive pulse sensing technology. ACS Nano 8 (9), 9003–9015.
- Park, H., Hwang, E., Jang, M., Yoon, C., 2020. Exposure assessment of elemental carbon, polycyclic aromatic hydrocarbons and crystalline silica at the underground excavation sites for top-down construction buildings. PLoS One 15 (9), e0239010.
- Perlson, E., Maday, S., Fu, M.-M., Moughamian, A.J., Holzbaur, E.L.F., 2010. Retrograde axonal transport: pathways to cell death? Trends Neurosci. 33 (7), 335–344.
- Peters, A., Herr, C., Bolte, G., Heutelbeck, A., Hornberg, C., Kraus, T., Lakes, T., Matzarakis, A., Novak, D., Reifegerste, D., Traidl-Hoffmann, C., Zeeb, H., Schneider, A., Hoffmann, B., 2023. Health protection and climate change require ambitious limit values for air pollutants in Europe: opinion on the revision of the directive on air quality and clean air for Europe of the environmental public health commission of the robert koch institute and the federal environment agency. Bundesgesundheitsblatt Gesundh. Gesundh. 66 (9), 1030–1034.
- Pohl, M.O., Violaki, K., Liu, L., Gaggioli, E., Glas, I., von Kempis, J., Messerli, C., Lin, C.-w, Terrettaz, C., David, S.C., Charlton, F.W., Motos, G., Bluvshtein, N., Schaub, A., Klein, L.K., Luo, B., Leemann, N.C., Ammann, M., Hugentobler, W., Krieger, U.K., Peter, T., Kohn, T., Nenes, A., Stertz, S., 2025. Comparative characterization of bronchial and nasal mucus reveals key determinants of influenza a virus inhibition. mSphere.
- Posit team (2025). RStudio: Integrated Development Environent for R. Posit Software, PBC, Boston, MA. URL http://www.posit.co/.
 Reisetter, A.C., Stebounova, L.V., Baltrusaitis, J., Powers, L., Gupta, A., Grassian, V.H.,
- Reisetter, A.C., Stebounova, L.V., Baltrusaitis, J., Powers, L., Gupta, A., Grassian, V.H., Monick, M.M., 2011. Induction of inflammasome-dependent pyroptosis by carbon black nanoparticles. J. Biol. Chem. 286 (24), 21844–21852.
- Roth, D., Sahin, A.T., Ling, F., Tepho, N., Senger, C.N., Quiroz, E.J., Calvert, B.A., van der Does, A.M., Guney, T.G., Glasl, S., van Schadewijk, A., von Schledorn, L., Olmer, R., Kanso, E., Nawroth, J.C., Ryan, A.L., 2025. Structure and function relationships of mucociliary clearance in human and rat airways. Nat. Commun. 16 (1), 2446.
- Schweinlin, M., Rossi, A., Lodes, N., Lotz, C., Hackenberg, S., Steinke, M., Walles, H., Groeber, F., 2017. Human barrier models for the in vitro assessment of drug delivery. Drug Deliv. Transl. Res 7 (2), 217–227.
- Shen, Y., Wu, L., Qin, D., Xia, Y., Zhou, Z., Zhang, X., Wu, X., 2018. Carbon black suppresses the osteogenesis of mesenchymal stem cells: the role of mitochondria. Part. Fibre Toxicol. 15 (1), 1–17.
- Sivarajan, R., Kessie, D.K., Oberwinkler, H., Pallmann, N., Walles, T., Scherzad, A., Hackenberg, S., Steinke, M., 2021. Susceptibility of human airway tissue models derived from different anatomical sites to bordetella pertussis and its virulence factor adenylate cyclase toxin. Front Cell Infect. Microbiol 11, 797491.
- Song, B., Liu, J., Feng, X., Wei, L., Shao, L., 2015. A review on potential neurotoxicity of titanium dioxide nanoparticles. Nanoscale Res. Lett. 10 (1).
- Stick, S., Bosco, A., Anderson, D., Iosifidis, T., Ling, K.-M., Wark, P., Kicic, A., Knight, D., 2017. A transcriptomic comparison between nasal and bronchial airway epithelia from childre. Eur. Respir. J. 50 (61), PA1826. PA1826.
- Stone, V., Miller, M.R., Clift, M.J.D., Elder, A., Mills, N.L., Moller, P., Schins, R.P.F., Vogel, U., Kreyling, W.G., Alstrup Jensen, K., Kuhlbusch, T.A.J., Schwarze, P.E., Hoet, P., Pietroiusti, A., De Vizcaya-Ruiz, A., Baeza-Squiban, A., Teixeira, J.P., Tran, C.L., Cassee, F.R., 2017. Nanomaterials versus ambient ultrafine particles: an opportunity to exchange toxicology knowledge. Environ. Health Perspect. 125 (10), 106002
- Tainio, M., Jovanovic Andersen, Z., Nieuwenhuijsen, M.J., Hu, L., de Nazelle, A., An, R., Garcia, L.M.T., Goenka, S., Zapata-Diomedi, B., Bull, F., Sá, T.H., 2021. Air pollution, physical activity and health: a mapping review of the evidence. Environ. Int 147, 105954.
- Tice, R.R., Agurell, E., Anderson, D., Burlinson, B., Hartmann, A, Kobayashi, H., Miyamae, Y., Rojas, E., Ryu, J.C, Sasaki, Y.F., 2000. Single cell gel/comet assay: guidelines for in vitro and in vivo genetic toxicology testing. Environ. mol. mutagen. 35 (3), 206–221.
- Turner, J.R., Rill, B.K., Carlson, S.L., Carnes, D., Kerner, R., Mrsny, R.J., Madara, J.L., 1997. Physiological regulation of epithelial tight junctions is associated with myosin light-chain phosphorylation. Am. J. Physiol. Cell Physiol. 273 (4), C1378–C1385.
- Vallabani, N.V.S., Gruzieva, O., Elihn, K., Juárez-Facio, A.T., Steimer, S.S., Kuhn, J., Silvergren, S., Portugal, J., Piña, B., Olofsson, U., Johansson, C., Karlsson, H.L., 2023. Toxicity and health effects of ultrafine particles: towards an understanding of the relative impacts of different transport modes. Environ. Res 231 (Pt 2), 116186.

Vermeer, P.D., Einwalter, L.A., Moninger, T.O., Rokhlina, T., Kern, J.A., Zabner, J., Welsh, M.J., 2003. Segregation of receptor and ligand regulates activation of enithelial growth factor recentor. Nature 422 (6929), 322–326.

epithelial growth factor receptor. Nature 422 (6929), 322–326.

World Health Organization, 2021. WHO global air quality guidelines: particulate matter (PM2.5 and PM10), ozone, nitrogen dioxide, sulfur dioxide and carbon monoxide.

World Health Organization, Geneva.

Yuksel, H., Turkeli, A., 2017. Airway epithelial barrier dysfunction in the pathogenesis and prognosis of respiratory tract diseases in childhood and adulthood. Tissue Barriers 5 (4), e1367458.